

Dynamical NNLO parton distributions

P. Jimenez-Delgado, E. Reya

*Universität Dortmund, Institut für Physik
D-44221 Dortmund, Germany*

Abstract

Utilizing recent DIS measurements ($\sigma_r, F_{2,3,L}$) and data on hadronic dilepton production we determine at NNLO (3-loop) of QCD the dynamical parton distributions of the nucleon generated radiatively from valencelike *positive* input distributions at an optimally chosen low resolution scale ($Q_0^2 < 1 \text{ GeV}^2$). These are compared with ‘standard’ NNLO distributions generated from positive input distributions at some *fixed* and higher resolution scale ($Q_0^2 > 1 \text{ GeV}^2$). Although the NNLO corrections imply in both approaches an improved value of χ^2 , typically $\chi_{\text{NNLO}}^2 \simeq 0.9\chi_{\text{NLO}}^2$, present DIS data are still not sufficiently accurate to distinguish between NLO results and the minute NNLO effects of a few percent, despite of the fact that the dynamical NNLO uncertainties are somewhat smaller than the NLO ones and both are, as expected, smaller than those of their ‘standard’ counterparts. The dynamical predictions for $F_L(x, Q^2)$ become perturbatively stable already at $Q^2 = 2 - 3 \text{ GeV}^2$ where precision measurements could even delineate NNLO effects in the very small- x region. This is in contrast to the common ‘standard’ approach but NNLO/NLO differences are here less distinguishable due to the larger 1σ uncertainty bands. Within the dynamical approach we obtain $\alpha_s(M_Z^2) = 0.1124 \pm 0.0020$, whereas the somewhat less constrained ‘standard’ fit gives $\alpha_s(M_Z^2) = 0.1158 \pm 0.0035$.

1 Introduction

Within the dynamical parton model approach the predicted small Bjorken- x behavior of structure functions is entirely due to QCD dynamics at $x \lesssim 10^{-2}$. This is due to the fact that the parton distributions at $Q^2 \gtrsim 1 \text{ GeV}^2$ are QCD radiatively generated from *valencelike* positive input distributions at an optimally determined low input scale $Q_0^2 \equiv \mu^2 < 1 \text{ GeV}^2$ (where ‘valencelike’ refers to $a_f > 0$ for *all* input distributions $xf(x, \mu^2) \propto x^{a_f}(1-x)^{b_f}$, i.e., not only the valence but also the sea and gluon input densities vanish at small x). Originally, its characteristic unique steep small- x predictions for the experimentally then unexplored region $x < 10^{-2}$ [1, 2, 3] were subsequently first confirmed in [4, 5]. With the advent of further high-precision data in recent years, the original dynamical parton distributions had to be updated [6, 7, 8] but the characteristic steep small- x behavior of the sea and the gluon distributions as $x \rightarrow 0$ remained essentially very similar.

Alternatively, in the common ‘standard’ approach, e.g. [9–21], the input scale is fixed at some *arbitrarily* chosen $Q_0 > 1 \text{ GeV}$ and the corresponding input distributions are less restricted. For example, the observed steep small- x behavior ($a_f < 0$) of the gluon and sea distributions has to be *fitted*, allowing even for negative gluon distributions [12, 13, 14, 18, 19], i.e. negative cross sections like a negative longitudinal structure function $F_L(x, Q^2)$. Furthermore the associated uncertainties encountered in the determination of the parton distributions turn out to be larger, particularly in the small- x region, than in the more restricted dynamical radiative approach where, moreover, the evolution distance (starting at $Q_0^2 < 1 \text{ GeV}^2$) is sizeably larger.

In the present paper we extend our most recent LO and NLO dynamical analysis [8] to the next-to-next-to-leading order (NNLO) of QCD. For consistency reasons we only consider deep inelastic scattering (DIS) and Drell–Yan dimuon production data where all required theoretical NNLO ingredients are available by now, except the ones for heavy

quark production. High- p_T hadron–hadron scattering processes will now not be considered since so far they are only known up to NLO. Furthermore we compare these ‘dynamical’ results for the radiatively generated parton distributions arising from a valencelike positive input at $Q_0 < 1$ GeV with the ones obtained from the common NNLO evolution approach being based on a ‘standard’ non–valencelike input at $Q_0 > 1$ GeV. In addition we shall analyze their associated uncertainties. Section 2 will be devoted to a discussion of some theoretical issues relevant for our NNLO analysis, in particular concerning our NNLO Q^2 -evolution algorithm for parton distributions, as well as of the relevant couplings and coefficient functions for relating them to the various neutral current structure functions required for calculating ‘reduced’ DIS cross sections. In Sect. 3 we present our quantitative results for structure functions, in particular our dynamical small- x predictions, and for hadronic dilepton production. The results related to the longitudinal structure $F_L(x, Q^2)$ are discussed in Sect. 4. Furthermore these dynamical results, together with their associated 1σ uncertainties, are compared with the ones obtained from a common ‘standard’ approach. Our conclusions are summarized in Sect. 5.

2 Evolutions of parton distributions and structure functions

Our NNLO analyses will be performed within the modified minimal subtraction ($\overline{\text{MS}}$) factorization and renormalization scheme. Heavy quarks (c, b, t) will not be considered as massless partons within the nucleon, i.e. the number of active (light) flavors n_f appearing in the splitting functions and the corresponding Wilson coefficients will be fixed, $n_f = 3$. This defines the so-called ‘fixed flavor number scheme’ (FFNS) which is fully predictive in the heavy quark sector where the heavy quark flavors are produced entirely perturbatively from the initial light (u, d, s) quarks and gluons – in full agreement with present experiments. Furthermore, in the evaluation of the running strong coupling $\alpha_s(Q^2)$ it is nevertheless

consistent and correct to utilize the standard variable n_f scheme for the β -function [22]. Up to NNLO, $a_s(Q^2) \equiv \alpha_s(Q^2)/4\pi$ evolves according to

$$da_s/d \ln Q^2 = - \sum_{k=0}^2 \beta_k a_s^{k+2} \quad (1)$$

where $\beta_0 = 11 - 2n_f/3$, $\beta_1 = 102 - 38n_f/3$ and $\beta_2 = 2857/2 - 5033n_f/18 + 325n_f^2/54$. Here we utilize the exact numerical (iterative) solution for $a_s(Q^2)$ since such an accuracy is mandatory, in particular at NNLO, in the low Q^2 region relevant for the valencelike approach [7, 8]. Since β_k is not continuous for different n_f , the continuity of $\alpha_s(Q^2)$ requires to match $\alpha_s^{(n_f)}$ at $Q = m_h$ ($h = c, b, t$), i.e., $\alpha_s^{(n_f)}(m_h) = \alpha_s^{(n_f-1)}(m_h)$. These naive matching conditions get corrected at NNLO [23, 24, 25] by a marginal term $-(11/72\pi^2)[\alpha_s^{(n_f-1)}(m_h)]^3$ which will be neglected. Furthermore we have chosen $m_c = 1.3$ GeV, $m_b = 4.2$ GeV and $m_t = 175$ GeV, which turned out to be the optimal choices for our NLO analysis of heavy quark production [8].

The Mellin n -moments of the parton distributions $f(x, Q^2)$,

$$f(n, Q^2) = \int_0^1 dx x^{n-1} f(x, Q^2) , \quad (2)$$

where $f = q, \bar{q}, g$, evolve according to

$$\frac{d\vec{q}(n, Q^2)}{d \ln Q^2} = \hat{P}(a_s, n)\vec{q}(n, Q^2) \quad (3)$$

which refers to the coupled flavor-*singlet* evolution equation for $\vec{q} = (\Sigma, g)^T$, $\Sigma = \sum_q (q + \bar{q})$, and

$$\hat{P}(a_s, n) = \sum_{k=0}^2 a_s^{k+1} \hat{P}_k(n) = \sum_{k=0}^2 a_s^{k+1} \begin{pmatrix} P_{qq}^{(k)} & P_{qg}^{(k)} \\ P_{gq}^{(k)} & P_{gg}^{(k)} \end{pmatrix} \quad (4)$$

with the well known LO and NLO splitting functions $P_{ij}^{(0)}$ and $P_{ij}^{(1)}$, respectively, and the NNLO (3-loop) $P_{ij}^{(2)}$ have been calculated in [26]. Any obvious Q^2 - and/or n -dependence will be suppressed as far as possible. The 2×2 matrix evolution equation (3) can be formally solved recursively [27, 28] with the result

$$\vec{q}(n, Q^2) = [\hat{L} + a_s \hat{U}_1 \hat{L} - a_{s0} \hat{L} \hat{U}_1 + a_s^2 \hat{U}_2 \hat{L} - a_s a_{s0} \hat{U}_1 \hat{L} \hat{U}_1 - a_{s0}^2 \hat{L} (\hat{U}_2 - \hat{U}_1^2)] \vec{q}(n, Q_0^2) \quad (5)$$

where $a_{s0} = \alpha_s(Q_0^2)/4\pi$. This is the so-called truncated solution where all redundant $\mathcal{O}(a_s^3)$ terms are disregarded. The LO evolution operator $\hat{L} = \hat{L}(a_s, a_{s0}, n)$, relevant for the LO solution $\vec{q}_{\text{LO}}(n, Q^2) = \hat{L}(a_s, a_{s0}, n)\vec{q}(n, Q_0^2)$, can be written as

$$\hat{L}(a_s, a_{s0}, n) \equiv \left(\frac{a_s}{a_{s0}}\right)^{-\hat{R}_0} = \hat{e}_- \left(\frac{a_s}{a_{s0}}\right)^{-\lambda_-} + \hat{e}_+ \left(\frac{a_s}{a_{s0}}\right)^{-\lambda_+} \quad (6)$$

where $\hat{R}_0 \equiv \hat{P}_0/\beta_0$ and with the projection matrices \hat{e}_\pm being given by

$$\hat{e}_\pm = \frac{1}{\lambda_\pm - \lambda_\mp} [\hat{R}_0 - \lambda_\mp \hat{1}] \quad (7)$$

where $\lambda_- (\lambda_+)$ denote the smaller (larger) eigenvalue of \hat{R}_0 ,

$$\lambda_\pm = \frac{1}{2\beta_0} [P_{qq}^{(0)} + P_{gg}^{(0)} \pm \sqrt{(P_{qq}^{(0)} - P_{gg}^{(0)})^2 + 4P_{qg}^{(0)} P_{gq}^{(0)}}], \quad (8)$$

i.e., $\hat{R}_0 = \lambda_- \hat{e}_- + \lambda_+ \hat{e}_+$. Furthermore

$$\hat{U}_{k=1,2} = -\frac{1}{k} \left(\hat{e}_- \hat{R}_k \hat{e}_- + \hat{e}_+ \hat{R}_k \hat{e}_+ \right) + \frac{\hat{e}_+ \hat{R}_k \hat{e}_-}{\lambda_- - \lambda_+ - k} + \frac{\hat{e}_- \hat{R}_k \hat{e}_+}{\lambda_+ - \lambda_- - k} \quad (9)$$

with $\hat{R}_{k=1,2} = \hat{R}_k + \sum_{i=1}^{k-1} \hat{R}_{k-i} \hat{U}_i$ and $\hat{R}_k = \hat{P}_k/\beta_0 - \sum_{i=1}^k \beta_i \hat{R}_{k-i}/\beta_0$. We have not performed any required matrix multiplication in (5) analytically, since such a procedure did not reduce the required computer time of the subsequent numerical analysis. Rather, we have performed all required matrix multiplications *entirely numerically*, using the n -moments of the NNLO splitting functions [26] $P_{ij}^{(2)}$ appearing in (4) together with the standard LO $P_{ij}^{(0)}$ and NLO $P_{ij}^{(1)}$ ones (see, e.g. [26]). The Bjorken- x space results $\vec{q}(x, Q^2)$ are finally obtained by performing numerically a contour integral around the singularities of $\vec{q}(n, Q^2)$ in (5) in the complex n -plane in the standard way (see, for example, [1, 28, 29]).

In the flavor-*nonsinglet* (NS) sector we have a simple (uncoupled) evolution equation which, in n -moment space, reads

$$\frac{dq_{\text{NS}}(n, Q^2)}{d \ln Q^2} = P_{\text{NS}}(a_s, n) q_{\text{NS}}(n, Q^2) \quad (10)$$

where, similarly to (4), $P_{\text{NS}}(a_s, n) = \sum_{k=0}^2 a_s^{k+1} P_{\text{NS}}^{(k)}(n)$ which refers to the NS splitting functions P_{NS}^\pm and P_{NS}^v (see, for example, [30, 31]). These splitting functions govern the evolution of the usual NS combinations of parton distributions with q_{NS} referring to $q_{\text{NS},3}^\pm = u^\pm - d^\pm$, $q_{\text{NS},8}^\pm = u^\pm + d^\pm - 2s^\pm$, etc., where $q^\pm = q \pm \bar{q}$, and $q_{\text{NS}}^v = \sum_q (q - \bar{q})$. The NNLO splitting functions $P_{\text{NS}}^{(2)}$ have been given in [31] where the well known LO $P_{\text{NS}}^{(0)}$ and NLO $P_{\text{NS}}^{(1)}$ ones can be found as well. Since no matrices are involved in the NS evolution equation (10), its solution can be easily inferred from the singlet solution (5) where now we have $U_1 = -R_1$ and $2U_2 = -R_2 - R_1U_1$ and thus

$$q_{\text{NS}}(n, Q^2) = \left[1 - (a_s - a_{s0})R_1 - \frac{1}{2}(a_s^2 - a_{s0}^2)(R_2 - R_1^2) - a_{s0}(a_s - a_{s0})R_1^2 \right] Lq_{\text{NS}}(n, Q_0^2) \quad (11)$$

with $R_k = P_{\text{NS}}^{(k)}/\beta_0 - \sum_{i=1}^k \beta_i R_{k-i}/\beta_0$ and $L = L(a_s, a_{s0}, n) = (a_s/a_{s0})^{-R_0}$. Again, $q_{\text{NS}}(x, Q^2)$ is obtained from a numerical Mellin–inversion of $q_{\text{NS}}(n, Q^2)$.

We have tested our singlet and nonsinglet evolution codes using the PEGASUS program [32] for generating the ‘truncated’ solutions together with the commonly used toy input of the Les Houches and HERA–LHC Workshops [33, 34]. For $10^{-7} < x < 0.9$ we achieved an agreement of up to four decimal places in most cases which is similar to the required high–accuracy benchmarks advocated in [33, 34].

As already mentioned at the beginning of this Section we employ for our analysis the FFNS and fix the number of active light flavors $n_f = 3$ in *all* splitting functions $P_{ij}^{(k)}$ and in the corresponding Wilson coefficients to be discussed below. In this factorization scheme only the light quarks (u, d, s) are genuine, i.e., massless partons within the nucleon, whereas the heavy ones (c, b, t) are not. This scheme is fully predictive in the heavy quark sector where the heavy quark flavors are produced entirely perturbatively from the initial light u, d, s quarks and gluons with the full heavy quark mass $m_{c,b,t}$ dependence taken into account in the production cross sections – as required experimentally [35, 36, 37, 38], in particular in the threshold region. However, even for very large values of Q^2 , $Q^2 \gg m_{c,b}^2$, these FFNS predictions up to NLO are in remarkable agreement [7, 8] with DIS data

and, moreover, are perturbatively stable despite the common belief that ‘non-collinear’ logarithms $\ln(Q^2/m_h^2)$ have to be resummed for $h = c, b, t$.

This somewhat questionable resummation of heavy quark mass effects using massless evolution equations, starting at the unphysical ‘thresholds’ $Q^2 = m_h^2$, is pursued in the so-called zero-mass ‘variable flavor number scheme’ (VFNS) where also the heavy quarks are taken to be massless partons within the nucleon with their distributions being generated, e.g. up to NLO, from the boundary conditions $h(x, m_h^2) = \bar{h}(x, m_h^2) = 0$. Hence this factorization scheme is characterized by increasing the number n_f of massless partons by one unit at $Q^2 = m_h^2$ starting from $n_f = 3$ at $Q^2 = m_c^2$, i.e., $c(x, m_c^2) = \bar{c}(x, m_c^2) = 0$. The matching conditions are fixed by general continuity relations [39, 40] at the respective ‘thresholds’ $Q^2 = m_h^2$. Thus the ‘heavy’ $n_f > 3$ quark distributions are perturbatively uniquely generated from the $n_f - 1$ ones via the massless renormalization group Q^2 -evolutions (see, e.g. [10,15]; a comparative qualitative and quantitative discussion of the zero-mass VFNS and the FFNS has been recently presented in [41]). Sometimes one uses an improvement on this, now known as the general-mass VFNS [11, 12, 13, 40, 42, 43, 44, 45, 46], where mass-dependent corrections are maintained in the hard cross sections. This latter factorization scheme interpolates between the zero-mass VFNS and the (experimentally required) FFNS used for our analysis.

In order to avoid any further dependence on model assumptions, we choose to work with experimentally directly measurable quantities, as has been done in [8], like the ‘reduced’ DIS one-photon exchange cross section $\sigma_r = F_2 - (y^2/Y_+)F_L$ together with the full neutral current (NC) cross sections [47]

$$\sigma_{r,\text{NC}}^{e^\pm p}(x, Q^2) = \left(\frac{2\pi\alpha^2 Y_+}{xQ^4} \right)^{-1} \frac{d^2\sigma_{\text{NC}}^{e^\pm p}}{dx dQ^2} = F_2^{\text{NC}} - \frac{y^2}{Y_+} F_L^{\text{NC}} \mp \frac{Y_-}{Y_+} x F_3^{\text{NC}} \quad (12)$$

where $\alpha = 1/137.036$, $Y_\pm = 1 \pm (1 - y)^2$ and

$$\begin{aligned} F_{2,L}^{\text{NC}} &= F_{2,L} - v_e \kappa F_{2,L}^{\gamma Z} + (v_e^2 + a_e^2) \kappa^2 F_{2,L}^Z \\ F_3^{\text{NC}} &= -a_e \kappa F_3^{\gamma Z} + 2v_e a_e \kappa^2 F_3^Z, \end{aligned} \quad (13)$$

with $v_e = -\frac{1}{2} + 2\sin^2\theta_W$, $a_e = -\frac{1}{2}$ and $\kappa^{-1} = 4\sin^2\theta_W \cos^2\theta_W(Q^2 + M_Z^2)/Q^2$, using $\sin^2\theta_W = 0.2312$ and $M_Z = 91.1876$ GeV. As in our previous NLO analysis [8] it turned out, however, that fitting just to the usual (one-photon exchange) $F_2(x, Q^2)$ gives rather similar results. Defining $\mathcal{F}_{2,L} \equiv F_{2,L}/x$, the n -moments in (2) of these structure functions $\mathcal{F}_{2,L}(x, Q^2)$ and $F_3(x, Q^2)$ can, for $n_f = 3$ light flavors, be written as

$$\begin{aligned}\mathcal{F}_{j=2,L}^{\text{NC}} &= C_{j,\text{NS}}(a_3^+ q_{\text{NS},3}^+ + a_8^+ q_{\text{NS},8}^+) + a^+(C_{j,q}\Sigma + C_{j,gg}) \\ F_3^{\text{NC}} &= C_{3,\text{NS}}(a^- q_{\text{NS}}^v + a_3^- q_{\text{NS},3}^- + a_8^- q_{\text{NS},8}^-)\end{aligned}\quad (14)$$

where $a_3^\pm = \frac{1}{2}(a_u^\pm - a_d^\pm)$, $a_8^\pm = \frac{1}{6}(a_u^\pm + a_d^\pm - 2a_s^\pm)$ and $a^\pm = \frac{1}{3}\sum_{q=u,d,s} a_q^\pm$ with

$$\begin{aligned}a_q^+ &= e_q^2 - 2e_q v_e v_q \kappa + (v_e^2 + a_e^2)\kappa^2 \\ a_q^- &= -2e_q a_q \kappa + 4v_e a_e v_q a_q \kappa^2\end{aligned}\quad (15)$$

where $v_q = \pm\frac{1}{2} - 2e_q \sin^2\theta_W$ and $a_q = \pm\frac{1}{2}$ with \pm according to whether q is a u - or d -type quark. The Wilson coefficients are generically expanded as [30, 48] $C_{2,3}(a_s, n) = \sum_{k=0}^2 a_s^k c_{2,3}^{(k)}(n)$ where at LO $c_{2,\text{NS}}^{(0)} = c_{2,q}^{(0)} = c_{3,\text{NS}}^{(0)} = 1$ and $c_{2,g}^{(0)} = 0$. The appropriate NLO (1-loop) coefficients $c_{2,3}^{(1)}$ can be found, for example, in [49]. The NNLO (2-loop) coefficients $c_{2,3}^{(2)}$ have been originally calculated in [50, 51] and, for definiteness, we take $c_{2,\text{NS}}^{(2)} \equiv c_{2,\text{NS}}^{(2)+}$, $c_{2,q}^{(2)}$ and $c_{2,g}^{(2)}$ from [52], and $c_{3,\text{NS}}^{(2)} \equiv c_{3,\text{NS}}^{(2)-}$ from [51]. Since the longitudinal structure function $F_L = F_2 - 2xF_1$ vanishes at LO, it has become common [50] to consider the first nonvanishing $\mathcal{O}(\alpha_s)$ contribution to F_L as the LO one, i.e., the perturbative expansion up to NNLO now reads $C_L(a_s, n) = \sum_{k=1}^3 a_s^k c_L^{(k)}(n)$. The relevant NNLO (3-loop) coefficients $c_L^{(3)}$ have been calculated in [52, 53], where also the well known LO $c_L^{(1)}$ and NLO $c_L^{(2)}$ coefficients can be found. Although we perform all calculations in Mellin n -moment space, it should be nevertheless mentioned that in Bjorken- x space the simple products in (14) turn into the standard convolutions of the Wilson coefficients with the parton distributions.

In the medium to large x -region the relevant kinematic nucleon target mass (TM) corrections are also taken into account for the dominant ‘light’ F_2 structure function in (14)

(with ‘light’ referring to the common u, d, s (anti-)quarks and gluon initiated contributions) according to [54]

$$\begin{aligned}
F_{2,\text{TM}}(n, Q^2) &\equiv \int_0^1 dx x^{n-2} F_{2,\text{TM}}(x, Q^2) \\
&= \sum_{\ell=0}^2 \left(\frac{m_N^2}{Q^2} \right)^\ell \frac{(n+\ell)!}{\ell!(n-2)!} \frac{F_2(n+2\ell, Q^2)}{(n+2\ell)(n+2\ell-1)} + \mathcal{O}\left(\left(\frac{m_N^2}{Q^2}\right)^3\right) \quad (16)
\end{aligned}$$

where higher powers than $(m_N^2/Q^2)^2$ are negligible for the relevant $x < 0.8$ region, as can straightforwardly be shown by comparing (16) with the well-known exact expression in Bjorken- x space [54].

So far we have discussed only the contributions of light partons (u, d, s, g) to structure functions in (14), $F_{i=2,L,3}^{\text{light}}$. The total structure functions $F_i(x, Q^2) = F_i^{\text{light}} + F_i^{\text{heavy}}$ require also the knowledge of the (subleading) heavy quark contribution $F_i^{\text{heavy}} = F_i^c + F_i^b$ at fixed-order of perturbation theory. (Top quark contributions are negligible.) The LO $\mathcal{O}(\alpha_s)$ contributions to $F_{2,L}^h$, due to the subprocess $\gamma^*g \rightarrow h\bar{h}$ with $h = c, b$, have been summarized in [6], and the NLO $\mathcal{O}(\alpha_s^2)$ ones are given in [55, 56]. The NNLO $\mathcal{O}(\alpha_s^3)$ 3-loop corrections to F_L^h and first rudimentary contributions to F_2^h have been calculated recently [57, 58, 59] for $Q^2 \gg m_h^2$, but these asymptotic results are neither applicable for our present investigation nor relevant for the majority of presently available data at lower values of Q^2 . Our ignorance of the full NNLO $\mathcal{O}(\alpha_s^3)$ corrections to $F_{2,L}^h$ constitute the major problem for any NNLO DIS analysis in the FFNS. (It should be mentioned that we have attempted to mimic the NNLO contributions by naively assuming them to be down by one power of α_s times the NLO terms multiplied by a constant K -factor, but the fit results were insensitive to such an ad hoc correction. However, this approach (guess) appears to be not appropriate since playing the same game at NLO, i.e., α_s times LO times a K -factor can not reproduce the correct NLO results in the relevant kinematic region of x and Q^2 .)¹ Therefore, the heavy flavor contributions $F_{2,L}^h$ are taken as given by fixed

¹A further (inconsistent) ‘check’ of the relevance of the unknown massive NNLO coefficient functions can be made by comparing the predicted charm and bottom structure functions using our new NNLO

order NLO perturbation theory [55, 56] as in our previous more restricted NNLO analyses [60, 61]. This is also common in the literature [15, 16, 17] and the error in the resulting parton distributions due to NNLO corrections to heavy quark production is expected [15] to be less than their experimental errors. These contributions are gluon $g(x, \mu_F^2)$ dominated and the factorization scale, also of the remaining parton distributions, should preferably be chosen [62] to be $\mu_F^2 = 4m_h^2$, although a much larger choice like $\mu_F^2 = 4(Q^2 + 4m_h^2)$ leaves the NLO results essentially unchanged [7, 8]. The NNLO heavy quark contributions to F_3^{NC} are not known either, but here they vanish in LO and are already negligibly small in NLO at the relevant large values of Q^2 as discussed in [8].

More recently the NNLO corrections to the rapidity distribution $d^2\sigma/dM dy$ of Drell–Yan (DY) dilepton production of mass M has been calculated as well [63, 64]. This allows to include DY data as well for performing a fully consistent analysis up to NNLO. Needless to say that the DY pp and pd dilepton production data are instrumental in fixing $\bar{d} - \bar{u}$ (or \bar{d}/\bar{u}). Only the usual high- p_T inclusive jet production data of hadron-hadron scattering have to be disregarded where the NNLO corrections have not yet been calculated. The LO and NLO corrections to the DY process are well known (for a summary, see, e.g., [65]) and for our full NNLO analysis we used the routine developed in [66] based on the results of [63, 64].

Finally, the evaluation of the uncertainties of our NNLO parton distributions is performed in the same way as of our recent NLO ones [8] which followed the line of [67, 68, 69]. The uncertainties $\Delta a_i = a_i - a_i^0$ of the central free fit parameters a_i^0 , corresponding to the minimal χ_0^2 , are constrained by $\Delta\chi^2 \leq T^2$ with the tolerance parameter T chosen to be $T^2 = T_{1\sigma}^2 = \sqrt{2N}/(1.65)^2 \simeq (4.5)^2$, i.e., T being slightly smaller than in [8] due to the smaller total number of data points considered, $N = 1568$, because the high- p_T jet data

(anti)quark and gluon distributions, as presented in Sec. 3, and the currently known massive NLO coefficient functions with the fully consistent NLO predictions (e.g. [8]) based on NLO parton distributions. These predictions turn out to be indistinguishable, except at very small values of x , $x \lesssim 10^{-4}$, where the ‘NNLO results’ are about 10-15% smaller than the NLO ones as shown for example in Figs. 8 and 9 of [8]. This is still fully consistent with the $c\bar{c}$ and $b\bar{b}$ HERA DIS data at very small x [35, 36, 37, 38].

and the DIS data for semi-inclusive $c\bar{c}$ - and $b\bar{b}$ -production cannot consistently be included in a global NNLO fit for the time being.

3 Quantitative results and dynamical small- x predictions

Now we extend our recent dynamical LO and NLO($\overline{\text{MS}}$) analysis [8] to NNLO($\overline{\text{MS}}$). The valencelike input distributions $xf(x, Q_0^2)$ at the input scale $Q_0 \equiv \mu < 1$ GeV, referring to the flavor nonsinglet (valence) densities $u_v, d_v, \Delta \equiv \bar{d} - \bar{u}$ and to the valencelike densities $\bar{d} + \bar{u}, \bar{s} = s$ and g in the singlet sector, are generically parametrized as

$$xf(x, Q_0^2) = N_f x^{a_f} (1-x)^{b_f} (1 + A_f \sqrt{x} + B_f x) , \quad (17)$$

subject to the constraints $\int_0^1 u_v dx = 2, \int_0^1 d_v dx = 1$ and

$$\int_0^1 x[u_v + d_v + 2(\bar{u} + \bar{d} + \bar{s}) + g]dx = 1 . \quad (18)$$

Since the data sets we are using are insensitive to the specific choice of the strange quark distributions, we continue to generate the strange densities entirely radiatively [7, 8] starting from $\bar{s}(x, Q_0^2) = s(x, Q_0^2) = 0$ in the dynamical valencelike approach where $Q_0 < 1$ GeV. For comparison we also study the common standard evolution approach, being based on a non-valencelike input at $Q_0 > 1$ GeV, where we choose as usual $\bar{s}(x, Q_0^2) = s(x, Q_0^2) = [\bar{u}(x, Q_0^2) + \bar{d}(x, Q_0^2)]/4$. Furthermore, since all our fits did not require the additional polynomial in (17) for the gluon distribution, we have set $A_g = B_g = 0$. This left us with a total of 21 independent fit parameters, including α_s . As suggested in [10] and done in our previous NLO analysis [8], we included in our final error analysis only those parameters that are actually sensitive to the input data set chosen, i.e. those parameters that are not close to ‘flat’ directions in the overall parameter space. With current data, and our functional form (17), 13 such parameters, including α_s , are included in our final error

analysis. The remaining highly correlated ill-determined eight polynomial parameters A_f and B_f , with uncertainties of more than 50%, were held fixed.

These free parameters have been fixed using the following data sets: the HERA ep measurements [70, 71, 72, 73, 74] for $Q^2 \geq 2 \text{ GeV}^2$ for the ‘reduced’ cross sections σ_r and $\sigma_{r,\text{NC}}$ in (12); the fixed target F_2^p data of SLAC [75], BCDMS [76], E665 [77] and NMC [78], subject to the standard cuts $Q^2 \geq 4 \text{ GeV}^2$ and $W^2 = Q^2(\frac{1}{x} - 1) + m_p^2 \geq 10 \text{ GeV}^2$, together with the structure function ratios F_2^n/F_2^p of BCDMS [79], E665 [80] and NMC [81]. Furthermore the Drell–Yan muon pair production data of E866/NuSea [82] for $d^2\sigma^{pN}/dM dx_F$ with $N = p, d$ have been used as well as their asymmetry measurements [83] for σ^{pd}/σ^{pp} . The DY data are always given in terms of x_F -distributions, whereas the NNLO expressions have been given in terms of the dilepton rapidity y -distributions [63, 64, 66]. Since experimentally the dilepton p_T is small (below about 1.5 GeV) as compared to the dilepton invariant mass $M \gtrsim 5 \text{ GeV}$, we have checked that it can be safely neglected and the two distributions can be related using leading order kinematics, as has been done in [17]: $d^2\sigma/dM dx_F = (x_1 + x_2)^{-1} d^2\sigma/dM dy$ where $x_{1,2} = (M^2/s)^{1/2} e^{\pm y}$, $x_F = x_1 - x_2$ and $x_1 + x_2 = (x_F^2 + 4M^2/s)^{1/2}$. All these data sets correspond to 1568 data points.

The parameters obtained from our NNLO dynamical fit for the input distributions at the optimal input scale $Q_0^2 \equiv \mu_{\text{NNLO}}^2 = 0.55 \text{ GeV}^2$ are given in Table 1, and the ones for our standard fit, corresponding to the choice $Q_0^2 = 2 \text{ GeV}^2$, in Table 2. Due to the fact that the higher the perturbative order the faster $\alpha_s(Q^2)$ increases as Q^2 decreases, a NNLO analysis is expected to result in a smaller value for $\alpha_s(M_Z^2)$ than a NLO fit in order to compensate for this increase. Our dynamical analysis indeed yields a smaller value at NNLO in Table 1, $\alpha_s^{\text{NNLO}}(M_Z^2) = 0.1124 \pm 0.0020$, as compared to our NLO fit [8] which resulted in $\alpha_s^{\text{NLO}}(M_Z^2) = 0.1145 \pm 0.0018$. Both values lie, however, within a 1σ uncertainty. (Similar results were obtained in a previous dynamical fit [61] which was performed for a restricted set of (mainly small- x) DIS data.) The same holds for our NNLO ‘standard’ fit result in Table 2, $\alpha_s^{\text{NNLO}}(M_Z^2) = 0.1158 \pm 0.0035$, to be compared with

the NLO result [8] of 0.1178 ± 0.0021 . Our standard NNLO fit result for $\alpha_s(M_Z^2)$ in Table 2 agrees, within errors, with the results of [15, 16] and [17], 0.1143 ± 0.0014 and 0.1128 ± 0.0015 , respectively, and is compatible with the one obtained from a ‘standard’ fit [60] to a restricted set of small- x DIS data. Data for high- p_T jet production in hadron-hadron scattering should not be included in a consistent NNLO analysis, since such processes are theoretically known only up to NLO. Including them nevertheless in a standard NNLO analysis requires [14, 84] generally larger values of $\alpha_s(M_Z^2)$. Previous standard NNLO fits ($Q_0 > 1$ GeV) considering only the flavor non-singlet (NS) valence sector of structure functions [85, 86, 87] resulted in somewhat smaller values of $\alpha_s(M_Z^2)$ than in Table 2 but remain within a $1\sigma - 2\sigma$ uncertainty. A similar NS valence analysis [88] as well as a full analysis [89] being based, however, on incomplete calculations of the moments of 3-loop anomalous dimensions (splitting functions) yielded slightly larger values of α_s at NNLO, $\alpha_s(M_Z^2) \simeq 0.117$, with estimated errors large enough so as to comply with our result in Table 2. For a more detailed and comparative recent discussion of NLO and NNLO results the interested reader is referred to [90]. In general, the NNLO fits result in a better (smaller) χ^2 than the NLO ones [8], typically $\chi_{\text{NNLO}}^2 \simeq 0.9\chi_{\text{NLO}}^2$.

It should be noticed that our α_s -uncertainty in Table 2 is about twice as large as the one obtained in a comparable standard NNLO analysis [17] where the high- p_T jet data have been disregarded for consistency reasons as well. Without these data the gluon distribution is little constrained in the medium to large x -region where it plays an important role for the Q^2 -evolution at small values of x due to the convolution with the dominant $P_{gg}^{(k)}$. This α_s -uncertainty remains sizeable irrespective of the choice of the input scale $Q_0 > 1$ GeV. Only within a Bayesian treatment of systematic errors, by taking into account point-to-point correlations [91, 92, 93], the uncertainty of $\alpha_s(M_Z^2)$ turns out to be about two times smaller [15, 16, 17, 91, 92, 93]. On the other hand the α_s -uncertainty of our dynamical fit in Table 1 is also about half as large as the ‘standard’ one in Table 2. Apart from the larger evolution distance, this is due to the strongly constrained valencelike input gluon

distribution $xg(x, Q_0^2) = N_g x^{a_g} (1-x)^{b_g}$ at $Q_0^2 = 0.55 \text{ GeV}^2$ in the small- x region where $a_g \simeq 1$, according to Table 1; consequently the energy-momentum sum rule (18) sufficiently constrains $xg(x, Q_0^2)$ in the medium to large x -region as we shall see below.

Our dynamical NNLO valence and valencelike (sea and gluon) input distributions at $Q_0^2 = \mu_{\text{NNLO}}^2 = 0.55 \text{ GeV}^2$ are shown in Fig. 1, according to the parameters in Table 1, together with their 1σ uncertainties. A comparison with our previous NLO results [8] (dashed curves) shows that u_v and d_v are now somewhat enhanced around $x = 0.1$ to 0.2 and that a strong and clear valencelike small- x behavior of the NNLO gluon input is now required, $a_g = 0.994 \pm 0.379$, as compared to $a_g \simeq 0.5168 \pm 0.4017$ at NLO [8]. Furthermore there is also a strong enhancement of the NNLO gluon over the NLO one around $x = 0.1$ and a sizeable depletion at larger values of x . The valence distributions of our standard analyses ($Q_0^2 = 2 \text{ GeV}^2$) are compared with the standard NNLO ones of Alekhin, Melnikov and Petriello [17] (AMP06, $Q_0^2 = 9 \text{ GeV}^2$) and the standard pure NS analysis of Blümlein, Böttcher and Guffanti [87] (BBG06, $Q_0^2 = 4 \text{ GeV}^2$) in Fig. 2 at $Q^2 = 4 \text{ GeV}^2$. In the relevant valence x -region, $x \gtrsim 0.1$, we confirm the NNLO BBG06 results, in particular the enhancement of xd_v with respect to the NNLO result of AMP06. In any case we, as well as BBG06, observe a significant enhancement of the NNLO xu_v and xd_v with respect to the NLO results. The valence distributions are very robust with respect to the choice of the input scale Q_0^2 since our dynamical valence distributions at $Q^2 = 4 \text{ GeV}^2$ practically coincide with the standard ones shown in Fig. 2.

The distinctive valencelike gluon input at low $Q^2 < 1 \text{ GeV}^2$ in Fig. 1 implies a far stronger constrained gluon distribution at larger values of Q^2 as compared to a gluon density obtained from a ‘standard’ fit with a conventional non-valencelike input at $Q^2 > 1 \text{ GeV}^2$, $Q_0^2 = 2 \text{ GeV}^2$ say, as can be seen in Fig. 3. In contrast to the standard NLO results [8] (shown by the dotted curves in Fig. 3) the standard NNLO gluon input at $Q_0^2 = Q^2 = 2 \text{ GeV}^2$ is very weakly constrained at small x ($a_g = 0.0637 \pm 0.1333$, cf. Table 2) and therefore (18) cannot sufficiently constrain it at larger values of x since, moreover,

high- p_T jet data have not been taken into account for consistency reasons. Notice that this common standard NNLO input gluon distribution at $Q_0^2 = 2 \text{ GeV}^2$ is also compatible with a valencelike small- x behavior ($a_g > 0$) — a tendency already observed in [13] — and that our dynamical NNLO gluon distribution in Fig. 3 (solid curves) remains valencelike even at $Q^2 = 2 \text{ GeV}^2$ (i.e. decreases with decreasing x). This is mainly caused by the NNLO splitting function $P_{gg}^{(2)}$ in (4) which is *negative* and *more* singular in the small- x region [26] than the LO and NLO ones: for $n_f = 3$, $xP_{gg}^{(2)}(x) \sim -3147.66 \ln \frac{1}{x} + 14737.89$ as $x \rightarrow 0$, whereas $xP_{gg}^{(0)}(x) \sim 12$ and $xP_{gg}^{(1)}(x) \sim -81.33$. The uncertainties generally decrease as Q^2 increases due to the QCD Q^2 -evolutions [67, 69], but the ones of the dynamical predictions in the small- x region remain substantially smaller than the uncertainties of the common ‘standard’ results as exemplified in Fig. 3. Furthermore, it is a general feature of *any* NNLO gluon distribution in the small- x region that it falls *below* the NLO one as can be seen in Fig. 3 by comparing the solid curves with the long-dashed ones, and the dashed-dotted curves with the dotted ones. In the first dynamical case the NNLO predictions for $x < 10^{-3}$ are several- σ below the NLO ones. For comparison we also display in Fig. 3 the standard NNLO results of AMP06 [17] based on an input scale $Q_0^2 = 9 \text{ GeV}^2$.

The dynamical sea distribution $x(\bar{u} + \bar{d})$ derives from a less pronounced ($a_{\bar{u}+\bar{d}} < a_g$) valencelike input in Fig. 1 which vanishes very slowly as $x \rightarrow 0$ ($a_{\bar{u}+\bar{d}} = 0.1374 \pm 0.0501$, cf. Table 1). This implies that the valencelike sea input is similarly increasing with decreasing x down to $x \simeq 0.01$ as the sea input obtained by the common standard fit where $a_{\bar{u}+\bar{d}} = -0.1098 \pm 0.0122$ according to Table 2. Therefore, the 1σ uncertainty bands of our dynamically predicted sea distributions at larger values of Q^2 in Fig. 4 are only marginally smaller than the corresponding ones of the standard fit. In contrast to the evolution of the gluon distribution in Fig. 3, the NNLO sea distributions in Fig. 4 lie always *above* the NLO ones in the small- x region, $x \lesssim 10^{-2}$, and at not too large values of Q^2 . Here all NNLO sea distributions are rather similar, including the ‘standard’ one of AMP06 [17].

A representative comparison of our dynamical and standard NNLO results with the

relevant HERA(H1,ZEUS) data on the proton structure function $F_2^p(x, Q^2)$ is presented in Figs. 5 and 6. It should be reemphasized that due to our valencelike input, the dynamical small- x results ($x \lesssim 10^{-2}$) are *predictions* being entirely generated by the QCD Q^2 -evolutions. This is in contrast to a common ‘standard’ fit where the gluon and sea input distributions in (17) do *not* vanish as $x \rightarrow 0$. For comparison we also display our dynamical NLO results [8] shown by the dashed curves. In all cases the data in Figs. 5 and 6 are well described throughout the whole medium- to small- x region for $Q^2 \gtrsim 2 \text{ GeV}^2$ and thus perturbative QCD is here fully operative. At $Q^2 < 2 \text{ GeV}^2$ the theoretical results fall below the data in the very small- x region; despite the fact that the NNLO results in Fig. 5 are closer to the data than the NLO ones, this is not unexpected for perturbative leading twist-2 results since nonperturbative (higher twist) contributions² to $F_2(x, Q^2)$ will eventually become relevant, even dominant, for decreasing values of Q^2 . Although the inclusion of NNLO corrections imply an improved value of χ^2 , typically $\chi_{\text{NNLO}}^2 \simeq 0.09\chi_{\text{NLO}}^2$ according to [8] and Tables 1 and 2, present high precision DIS data are not sufficiently accurate to distinguish between the NLO results and the minute NNLO effects of a few percent. This is illustrated in Fig. 7 where the experimental (statistical and systematic) errors are far bigger than the differences between the NLO and NNLO results. It should, however, be noticed that the NNLO 1σ uncertainty band is somewhat narrower (reduced) than the one at NLO. The results are similar for our ‘standard’ fits. It has already been noticed that, by analyzing only the flavor non-singlet valence sector of structure functions, NNLO effects cannot be delineated by present data in the medium- to large- x region, and moreover, uncertainties of NLO and LO analyses (such as higher twists, different factorization schemes and QED contributions to the QCD Q^2 -evolutions) turn out to be comparable in size to the NNLO 3-loop contributions [86].

As already pointed out, the measurements of Drell–Yan dilepton production in pp and

²Since operators of different twists do *not* mix under renormalization group evolutions, possible higher-twist effects do not influence the determination of the input parameters at the low input scale $Q_0^2 = 0.55 \text{ GeV}^2$ relevant for the dynamical (valencelike) leading twist-2 distributions, with the latter being determined from data at $Q^2 \geq 2 \text{ GeV}^2$ and $Q^2 \geq 4 \text{ GeV}^2$ with $W^2 \geq 10 \text{ GeV}^2$ as discussed above.

pd collisions [82, 83] are instrumental in fixing $\Delta \equiv \bar{d} - \bar{u}$ (or \bar{d}/\bar{u}) [94]. In Figs. 8 and 9 we display our dynamical NNLO and NLO results, together with the $\pm 1\sigma$ uncertainties, for the differential dimuon mass distributions for various average values of $x_F = x_1 - x_2$ for pp and pd collisions, respectively. The ‘standard’ fit results differ only marginally. In the relevant kinematic region where high–statistics data exist, all three NNLO and NLO results shown agree within 1σ . In Fig. 10 we show the result for the ratio $\sigma^{pd}/2\sigma^{pp}$ relevant for the DY asymmetry $A_{DY} = (\sigma^{pp} - \sigma^{pn})/(\sigma^{pp} + \sigma^{pn})$. Notice that $\sigma^{pN} \equiv d^2\sigma^{pN}/dMdx_F \propto \sum_{u,d,s} e_q^2 [q(x_1)\bar{q}(x_2) + q(x_2)\bar{q}(x_1)]$ in LO at a scale $Q^2 \equiv M^2$, where x_1 and x_2 refer to the fractional momenta of the quarks in the beam (p) and the nucleon target (N), respectively. Experimentally $x_F > 0$ ($x_1 > x_2$) and consequently the Drell–Yan cross section is dominated by the annihilation of a beam quark with a target antiquark.

4 The longitudinal structure function $F_L(x, Q^2)$

As discussed in Sect. 2 we have explicitly used for our analysis the experimentally directly measured ‘reduced’ DIS cross sections (12) which, for not too large values of Q^2 , are dominated by the one–photon exchange cross section $\sigma_r = F_2 - (y^2/Y_+)F_L$ where $y = Q^2/xs$. The importance of using this quantity has been emphasized in [95]: the effect of F_L becomes increasingly relevant as x decreases at a given Q^2 , where y increases. This is seen in the data as a flattening of the growth of $\sigma_r(x, Q^2)$ as x decreases to very small values, at fixed Q^2 , leading eventually to a turnover (cf. Fig. 11). At lower values of Q^2 in Fig. 11 it was not possible in [95] to reproduce this turnover at NLO. This was mainly due to the negative longitudinal cross section (negative $F_L(x, Q^2)$) encountered in [13, 95]. Since all of our cross sections and subsequently all structure functions are manifestly positive throughout the whole kinematic region considered, our dynamical NLO [8] and NNLO results in Fig. 11 are in good agreement with all small– x HERA measurements [70–74].

The same holds true for our ‘standard’ NLO [8] and NNLO results which, besides having slightly wider uncertainty bands, are almost indistinguishable from the dynamical ones shown in Fig. 11. In Fig. 12 we display our NNLO results for σ_r at different proton beam energies E_p , relevant for most recent H1 measurements [96], where the turnover at small x becomes more pronounced at smaller energies because of the larger values of y . Our dynamical small- x predictions are fully compatible with the (preliminary) H1 data presented in [96].

Turning now to F_L itself we note that the n -moment equation (14) for F_L becomes in Bjorken- x space

$$x^{-1}F_L(x, Q^2) = C_{L,NS} \otimes \left(\frac{1}{6} q_{NS,3}^+ + \frac{1}{18} q_{NS,8}^+ \right) + \frac{2}{9} (C_{L,q} \otimes \Sigma + C_{L,g} \otimes g) + x^{-1}F_L^{\text{heavy}}(x, Q^2) \quad (19)$$

where \otimes in the light parton sector denotes the common convolution, and the weak Z^0 contributions in (13) and (15) have been neglected for $Q^2 \ll M_Z^2$ relevant for our present interest. We have also added the heavy quark (charm, bottom) contribution F_L^{heavy} for which we use, as discussed in Sect. 2, the NLO(2-loop) expressions also in NNLO due to our ignorance of the $\mathcal{O}(\alpha_s^3)$ NNLO heavy quark corrections. (This inconsistency is here of minor importance since F_L^c – and even more so F_L^b – is a genuinely subdominant NLO contribution to the total F_L , which holds of course also at LO (cf. Figs. 13 and 14)). Following the notation of Sect. 2, the perturbative expansion up to NNLO of the coefficient functions in (19) reads $C_{L,i}(\alpha_s, x) = \sum_{k=1}^3 a_s^k c_{L,i}^{(k)}(x)$. In LO, $c_{L,NS}^{(1)} = \frac{16}{3}x$, $c_{L,ps}^{(1)} = 0$, $c_{L,g}^{(1)} = 24x(1-x)$ and the flavor-singlet quark coefficient function is decomposed into the non-singlet and ‘pure singlet’ contribution, $c_{L,q}^{(k)} = c_{L,NS}^{(k)} + c_{L,ps}^{(k)}$. Sufficiently accurate simplified expressions for the NLO [97, 98, 99] and NNLO [52] coefficient functions $c_{L,i}^{(2)}$ and $c_{L,i}^{(3)}$, respectively, have been given in [53]. It has been furthermore noted in [53] that especially for $C_{L,g}$ both NLO and NNLO contributions are rather large over almost the entire x -range. Most striking, however, is the behavior of both singlet coefficient functions $C_{L,q}$ and $C_{L,g}$ in (19) at very small values of x : the vanishingly small LO parts ($xc_{L,i}^{(1)} \sim x^2$) are negligible

as compared to the negative constant NLO 2-loop terms, which in turn are completely overwhelmed by the *positive* NNLO 3-loop singular contribution $xc_{L,i}^{(3)} \sim \ln \frac{1}{x}$. This latter singular correction might be indicative for a perturbative instability at NNLO [53] but it should be kept in mind that a small- x information alone is *insufficient* for reliable estimates of the convolutions occurring in (19) when evaluating physical observables.

Our dynamical LO, NLO and NNLO predictions for the total F_L are displayed in Fig. 13, together with the small subdominant charm contributions at LO and NLO. These predictions become perturbatively stable already at $Q^2 \gtrsim 3 \text{ GeV}^2$ where the gluon contribution becomes dominant and where precision measurements could even delineate NNLO effects in the very small- x region. It should be noted that the error bands at smaller values of Q^2 (where the gluon and quark contributions are still comparable) are rather small. This is caused by compensating effects in the error analysis, although the individual light quark and gluon contributions have wider error bands. Within the common ‘standard’ approach the absolute values of the NNLO and NLO results in Fig. 14 differ by more at smaller Q^2 than the dynamical ones, but the differences between the NNLO and NLO results are here less distinguishable due to the larger 1σ uncertainty bands which partly overlap in the very small- x region. It should, however, be noted that it is somewhat deceptive to compare the error bands in Figs. 13 and 14: in the ‘dynamical’ approach (Fig. 13) the errors are strongly reduced due to the evolution from about 0.5 GeV^2 , in contrast to the much smaller evolution distances in the ‘standard’ approach (Fig. 14) where the evolution starts at the input scale $Q_0^2 = Q^2 = 2 \text{ GeV}^2$. It should furthermore be noticed that the NLO/NNLO instabilities implied by the standard fit results obtained in [13, 95] at $Q^2 \lesssim 5 \text{ GeV}^2$ are far more violent than the ones shown in Fig. 14 which is mainly due to the negative longitudinal cross section (negative $F_L(x, Q^2)$) encountered in [13, 95]. The perturbative stability in any scenario becomes in general better the larger Q^2 , typically beyond $4 - 5 \text{ GeV}^2$ [13, 53, 61, 95], as evident from Figs. 13 and 14. This is due to the fact that the Q^2 -evolutions eventually force any parton distribution to become sufficiently

steep in x . It should be mentioned that the sizeable discrepancies between NNLO and NLO predictions at $Q^2 = 2 \text{ GeV}^2$ and $x \simeq 10^{-5}$ in Figs. 13 and 14 are not too surprising since $Q^2 \simeq 2 \text{ GeV}^2$ represents somehow a borderline value for the leading twist-2 contribution to become dominant at small- x values. This is further corroborated by the observation that the dynamical NNLO and NLO twist-2 fits slightly undershoot the HERA data for F_2 at $Q^2 \lesssim 2 \text{ GeV}^2$ in the small- x region (cf. Fig. 5), which indicates that nonperturbative (higher twist) contributions² to structure functions become relevant for $Q^2 \lesssim 2 \text{ GeV}^2$ [7, 8].

For completeness we finally compare in Fig. 15 our NNLO dynamical and standard (leading twist) predictions for $F_L(x, Q^2)$, together with their $\pm 1\sigma$ error bands, with a representative selection of (partly preliminary) H1 data [72, 73, 100, 101, 102] at fixed $W \simeq 276 \text{ GeV}$. For comparison we also show in Fig. 15 our NLO results [8] which have 1σ uncertainty bands similar to the NNLO ones. All our NNLO and NLO results for F_L , being gluon dominated in the small- x region, are in full agreement with present measurements which is in contrast to expectations [12, 13, 95] based on negative parton distributions and structure functions at small values of x . To illustrate the manifest positive definiteness of our dynamically generated structure functions at $Q^2 \geq \mu^2$ ($\mu_{\text{NNLO}}^2 = 0.55 \text{ GeV}^2$, $\mu_{\text{NLO}}^2 = 0.5 \text{ GeV}^2$), we show $F_L(x, Q^2)$ in Fig. 15 down to small values of Q^2 although leading twist-2 predictions need not necessarily be confronted with data below, say, 2 GeV^2 .

5 Summary and conclusions

Utilizing recent DIS structure function measurements ($F_{2,3,L}$ and the ‘reduced’ cross section σ_r) and hadronic Drell–Yan dilepton production data, our previous LO and NLO global fit analyses for the dynamical parton distributions of the nucleon [8] have been extended to NNLO of perturbative QCD. The small- x ($x \lesssim 10^{-2}$) structure of dynamical parton distributions is generated entirely radiatively from *valencelike*, manifestly *positive*, input distributions at an optimally chosen input scale $Q_0^2 < 1 \text{ GeV}^2$. The NNLO predictions are

perturbatively stable with respect to the NLO ones and are in agreement with all present measurements for $Q^2 \gtrsim 2 \text{ GeV}^2$. In general, the NNLO corrections imply an improved value of χ^2 , typically $\chi_{\text{NNLO}}^2 \simeq 0.9 \chi_{\text{NLO}}^2$. Having augmented our analyses with an appropriate uncertainty analysis, it turned out that present DIS precision data are still not sufficiently accurate to distinguish between NLO results and the minute NNLO effects of a few percent, despite of the fact that the dynamical NNLO 1σ uncertainties are somewhat smaller than the NLO ones. Inclusive high- p_T jet data were disregarded for consistency reasons, since NNLO corrections have not yet been calculated. Nevertheless the *valencelike* input gluon distribution remains sufficiently constrained, via the energy-momentum sum rule, also at larger values of x (which is in contrast to a common ‘standard’ fit approach). It is interesting to note that our dynamical NNLO gluon distribution remains valencelike even at $Q^2 = 2 - 3 \text{ GeV}^2$ (i.e. decreases with decreasing x , cf. Fig. 3) which is mainly caused by the dominant NNLO gluon-gluon splitting function $P_{gg}^{(2)}$ which is negative and more singular as $x \rightarrow 0$ than the LO and NLO ones, $P_{gg}^{(2)}(x) \sim -\frac{1}{x} \ln \frac{1}{x}$. The drawback of any precision NNLO analysis at present is that the experimentally required heavy quark mass effects of heavy quark (charm, bottom) contributions can only be taken into account up to NLO because of our ignorance of the full NNLO $\mathcal{O}(\alpha_s^3)$ corrections.

Our dynamical distributions and predictions have also been compared with conventional (‘standard’) NNLO ones obtained from *non-valencelike* positive definite input distributions at some arbitrarily chosen higher input scale $Q_0^2 > 1 \text{ GeV}^2$. For this purpose we have performed a common ‘standard’ fit as well, assuming $Q_0^2 = 2 \text{ GeV}^2$ (notice that, contrary to the dynamical approach, the finite small- x behavior of the input gluon and sea distributions is here fitted, and *not* dynamically generated by QCD evolutions). As in the dynamical approach, the NNLO corrections imply here also an improved χ^2 , typically $\chi_{\text{NNLO}}^2 \simeq 0.9 \chi_{\text{NLO}}^2$. The 1σ uncertainties of these less constrained ‘standard’ distributions are, as expected, larger than those of their dynamical counterparts, in particular in the small- x region.

Our predictions for the longitudinal structure $F_L(x, Q^2)$ and results for the ‘reduced’ DIS cross section $\sigma_r(x, Q^2)$ are in agreement with all HERA data and most recent HERA–H1 measurements, in particular in the small– x region and down to $Q^2 = 2 \text{ GeV}^2$. The dynamical NNLO/NLO predictions for $F_L(x, Q^2)$ become perturbatively stable already at $Q^2 = 2 - 3 \text{ GeV}^2$ where future precision measurements could even delineate NNLO effects in the very small– x region (the NNLO 1σ uncertainty bands are here smaller than the NLO ones). This is in contrast to the common ‘standard’ approach but NNLO/NLO instabilities and differences are here less distinguishable due to the much larger 1σ error bands.

The strong coupling obtained from our dynamical NNLO analysis is $\alpha_s^{\text{NNLO}}(M_Z^2) = 0.1124 \pm 0.0020$ to be compared with $\alpha_s^{\text{NLO}}(M_Z^2) = 0.1145 \pm 0.0018$ at NLO [8]. The less constrained ‘standard’ approach at NNLO resulted in $\alpha_s^{\text{NNLO}}(M_Z^2) = 0.1158 \pm 0.0035$ to be compared with $\alpha_s^{\text{NLO}}(M_Z^2) = 0.1178 \pm 0.0021$ at NLO [8].

For our analysis in the ‘fixed flavor number scheme’ with $n_f = 3$ active light (u, d, s) flavors, we have developed our own (entirely numerical) NNLO Q^2 –evolution algorithm which has been tested by reproducing the appropriate Les Houches and HERA–LHC high–accuracy benchmarks [33, 34]. A FORTRAN code (grid) containing our NNLO dynamical and ‘standard’ light ($u, d, s; g$) parton distributions can be obtained on request or directly from <http://doom.physik.uni-dortmund.de/pdfserver>.

Acknowledgements

We thank very much S.I. Alekhin for providing us with a routine for calculating the NNLO corrections to the rapidity distribution of Drell–Yan dilepton production, as well as for a clarifying correspondence, and J. Blümlein for a helpful correspondence. We are very indebted to M. Glück for many discussions and for his continued interest. This work has been supported in part by the ‘Bundesministerium für Bildung und Forschung’, Berlin/Bonn.

References

- [1] M. Glück, E. Reya, A. Vogt, Z. Phys. C **48**, 471 (1990)
- [2] M. Glück, E. Reya, A. Vogt, Z. Phys. C. **53**, 127 (1992)
- [3] M. Glück, E. Reya, A. Vogt, Phys. Lett. B **306**, 391 (1993)
- [4] H1 Collaboration, I. Abt et al., Nucl. Phys. B **407**, 515 (1993)
- [5] ZEUS Collaboration, M. Derrick et al., Phys. Lett. B **316**, 412 (1993)
- [6] M. Glück, E. Reya, A. Vogt, Z. Phys. C **67**, 433 (1995)
- [7] M. Glück, E. Reya, A. Vogt, Eur. Phys. J. C **5**, 461 (1998)
- [8] M. Glück, P. Jimenez-Delgado, E. Reya, Eur. Phys. J. C **53**, 355 (2008)
- [9] CTEQ5 Collaboration, H.L. Lai et al., Eur. Phys. J. C **12**, 375 (2000)
- [10] CTEQ6 Collaboration, J. Pumplin et al., JHEP **0207**, 012 (2002)
- [11] CTEQ6.5 Collaboration, W.K. Tung et al., JHEP **0702**, 053 (2007)
- [12] A.D. Martin, R.G. Roberts, W.J. Stirling, R.S. Thorne, Eur. Phys. J. C **23**, 73 (2002)
- [13] A.D. Martin, R.G. Roberts, W.J. Stirling, R.S. Thorne, Phys. Lett. B **531**, 216 (2002)
- [14] A.D. Martin, W.J. Stirling, R.S. Thorne, G. Watt, Phys. Lett. B **652**, 292 (2007)
- [15] S.I. Alekhin, Phys. Rev. D **68**, 014 002 (2003)
- [16] S.I. Alekhin, JETP Lett. **82**, 628 (2005)
- [17] S.I. Alekhin, K. Melnikov, F. Petriello, Phys. Rev. D **74**, 054 033 (2006)
- [18] ZEUS Collaboration, J. Breitweg et al., Eur. Phys. J. C **7**, 609 (1999)

- [19] ZEUS Collaboration, S. Chekanov et al., Phys. Rev. D **67**, 012 007 (2003)
- [20] H1 Collaboration, C. Adloff et al., Eur. Phys. J. C **21**, 33 (2001)
- [21] H1 Collaboration, C. Adloff et al., Eur. Phys. J. C **30**, 1 (2003)
- [22] M. Glück, E. Reya, Mod. Phys. Lett. A **22**, 351 (2007)
- [23] W. Bernreuther, W. Wetzel, Nucl. Phys. B **197**, 228 (1982) [Erratum ibid. **513**, 758 (1998)]
- [24] S.A. Larin, T. van Ritbergen, J.A.M. Vermaseren, Nucl. Phys. B **438**, 278 (1995)
- [25] K.G. Chetyrkin, B.A. Kniehl, M. Steinhauser, Phys. Rev. Lett. **79**, 2184 (1997)
- [26] A. Vogt, S. Moch, J.A.M. Vermaseren, Nucl. Phys. B **691**, 129 (2004)
- [27] R.K. Ellis, Z. Kunszt, E. Levin, Nucl. Phys. B **420**, 517 (1994) [Erratum ibid. **433**, 498 (1995)]
- [28] J. Blümlein, A. Vogt, Phys. Rev. D **58**, 014 020 (1998)
- [29] D. Graudenz, M. Hampel, A. Vogt, C. Berger, Z. Phys. C **70**, 77 (1996)
- [30] W.L. van Neerven, A. Vogt, Nucl. Phys. B **568**, 263 (2000)
- [31] S. Moch, J.A.M. Vermaseren, A. Vogt, Nucl. Phys. B **688**, 101 (2004)
- [32] A. Vogt, Comput. Phys. Commun. **170**, 65 (2005)
- [33] S. Alekhin et al., QCD/SM Working Group Report of the workshop ‘Physics at the TeV Colliders’, Les Houches, May 2001 (hep-ph/0204316)
- [34] S. Alekhin et al., Working Group I: Parton Distributions, Summary Report for the HERA-LHC Workshop Proceedings, CERN-DESY 2004/2005 (hep-ph/0511119)
- [35] ZEUS Collaboration, S. Chekanov et al., Phys. Rev. D **69**, 012 004 (2004)

- [36] H1 Collaboration, C. Adloff et al., Phys. Lett. B **528**, 199 (2002)
- [37] H1 Collaboration, A. Aktas et al., Eur. Phys. J. C **40**, 349 (2005)
- [38] H1 Collaboration, A. Aktas et al., Eur. Phys. J. C **45**, 23 (2006)
- [39] J.C. Collins, W.K. Tung, Nucl. Phys. B **278**, 934 (1986)
- [40] M. Buza, Y. Matiounine, J. Smith, W.L. van Neerven, Eur. Phys. J. C **1**, 301 (1998)
- [41] M. Glück, P. Jimenez-Delgado, E. Reya, C. Schuck, Phys. Lett. B **664**, 133 (2008)
- [42] S. Kretzer et al., Phys. Rev. D **69**, 114 005 (2004)
- [43] M.A.G. Aivazis et al., Phys. Rev. D **50**, 3102 (1994)
- [44] A. Chuvakin, J. Smith, W.L. van Neerven, Phys. Rev. D **61**, 096 004 (2000)
- [45] R.S. Thorne, R.G. Roberts, Phys. Rev. D **57**, 6871 (1998)
- [46] R.S. Thorne, Phys. Rev. D **73**, 054 019 (2006)
- [47] M. Klein, T. Riemann, Z. Phys. C **24**, 151 (1984)
- [48] W.L. van Neerven, A. Vogt, Nucl. Phys. B **588**, 345 (2000)
- [49] W. Furmanski, R. Petronzio, Z. Phys. C **11**, 293 (1982)
- [50] E.B. Zijlstra, W.L. van Neerven, Nucl. Phys. B **383**, 525 (1992)
- [51] E.B. Zijlstra, W.L. van Neerven, Phys. Lett. B **297**, 377 (1992)
- [52] J.A.M. Vermaseren, A. Vogt, S. Moch, Nucl. Phys. B **724**, 3 (2005)
- [53] S. Moch, J.A.M. Vermaseren, A. Vogt, Phys. Lett. B **606**, 123 (2005)
- [54] H. Georgi, H.D. Politzer, Phys. Rev. D **14**, 1829 (1976)

- [55] E. Laenen et al., Nucl. Phys. B **392**, 162 (1993)
- [56] S. Riemersma, J. Smith, W.L. van Neerven, Phys. Lett. B **347**, 143 (1995)
- [57] J. Blümlein et al., Nucl. Phys. B **755**, 272 (2006)
- [58] I. Bierenbaum, J. Blümlein, S. Klein, Acta Phys. Pol. B **38**, 3543 (2007)
- [59] I. Bierenbaum, J. Blümlein, S. Klein, C. Schneider, Nucl. Phys. B **803**, 1 (2008)
- [60] M. Glück, C. Pisano, E. Reya, Eur. Phys. J. C **50**, 29 (2007)
- [61] M. Glück, C. Pisano, E. Reya, Phys. Rev. D **77**, 074 002 (2008) [Erratum ibid. **78**, 019 902 (2008)]
- [62] M. Glück, E. Reya, M. Stratmann, Nucl. Phys. B **422**, 37 (1994)
- [63] C. Anastasiou, L. Dixon, K. Melnikov, F. Petriello, Phys. Rev. Lett. **91**, 182 002 (2003)
- [64] C. Anastasiou, L. Dixon, K. Melnikov, F. Petriello, Phys. Rev. D **69**, 094 008 (2004)
- [65] P.J. Sutton et al., Phys. Rev. D **45**, 2349 (1992)
- [66] S.I. Alekhin, private communication
- [67] J. Pumplin et al., Phys. Rev. D **65**, 014 013 (2002)
- [68] J. Pumplin, D.R. Stump, W.K. Tung, Phys. Rev. D **65**, 014 011 (2002)
- [69] A.D. Martin et al., Eur. Phys. J. C **28**, 455 (2003)
- [70] H1 Collaboration, C. Adloff et al, Eur. Phys. J. C **13**, 609 (2000)
- [71] H1 Collaboration, C. Adloff et al., Eur. Phys. J. C **19**, 269 (2001)
- [72] H1 Collaboration, C. Adloff et al., Eur. Phys. J. C **21**, 33 (2001)

- [73] H1 Collaboration, C. Adloff et al., *Eur. Phys. J. C* **30**, 1 (2003)
- [74] ZEUS Collaboration, S. Chekanov et al., *Eur. Phys. J. C* **21**, 443 (2001)
- [75] L.W. Whitlow et al., *Phys. Lett. B* **282**, 475 (1992)
- [76] BCDMS Collaboration, A.C. Benvenuti et al., *Phys. Lett. B* **223**, 485 (1989)
- [77] E665 Collaboration, M.R. Adams et al., *Phys. Rev. D* **54**, 3006 (1996)
- [78] NMC Collaboration, M. Arneodo et al., *Nucl. Phys. B* **483**, 3 (1997)
- [79] BCDMS Collaboration, A.C. Benvenuti et al., *Phys. Lett. B* **237**, 599 (1990)
- [80] E665 Collaboration, M.R. Adams et al., *Phys. Rev. Lett.* **75**, 1466 (1995)
- [81] NMC Collaboration, M. Arneodo et al., *Nucl. Phys. B* **487**, 3 (1997)
- [82] E866/NuSea Collaboration, J. Webb, P.E. Reimer, hep-ex/0302019 (private communication)
- [83] E866/NuSea Collaboration, R.S. Towell et al., *Phys. Rev. D* **64**, 052 002 (2001)
- [84] A.D. Martin et al., *Phys. Lett. B* **604**, 61 (2004)
- [85] J. Blümlein, H. Böttcher, A. Guffanti, *Nucl. Phys. B (Proc. Suppl.)* **135**, 152 (2004)
- [86] M. Glück, E. Reya, C. Schuck, *Nucl. Phys. B* **754**, 178 (2006)
- [87] J. Blümlein, H. Böttcher, A. Guffanti, *Nucl. Phys. B* **774**, 182 (2007)
- [88] A.L. Kataev et al., *Phys. Lett. B* **417**, 374 (1998)
- [89] J. Santiago, F.J. Yndurain, *Nucl. Phys. B* **563**, 45 (1999)
- [90] J. Blümlein, Proceedings of the 15th Intl. Workshop on Deep Inelastic Scattering and Related Subjects (DIS 2007), Munich, 2007, Vol. 2, p. 1099 (arXiv: 0706.2430)

- [91] S.I. Alekhin, arXiv: hep-ex/0005042
- [92] S.I. Alekhin, Phys. Rev. D **63**, 094022 (2001)
- [93] S.I. Alekhin, Phys. Lett. B **519**, 57 (2001)
- [94] P.E. Reimer, J. Phys. G **34**, S107 (2007)
- [95] A.D. Martin, W.J. Stirling, R.S. Thorne, Phys. Lett. B **635**, 305 (2006)
- [96] H1 Collaboration, F.D. Aaron et al., Phys. Lett. B **665**, 139 (2008)
- [97] D.I. Kazakov, A.V. Kotikov, Nucl. Phys. B **307**, 721 (1988) [Erratum ibid. **345**, 299 (1990)]
- [98] J. Sanchez Guillen et al., Nucl. Phys. B **353**, 337 (1991)
- [99] E.B. Zijlstra, W.L. van Neerven, Phys. Lett. B **273**, 476 (1991)
- [100] H1 Collaboration, C. Adloff et al., Phys. Lett. B **393**, 452 (1997)
- [101] H1 Collaboration, E.M. Lobodzinska, Acta Phys. Pol. B **35**, 223 (2004), arXiv:hep-ph/0311180
- [102] T. Lastovicka, Eur. Phys. J. C **33**, s388 (2004)

	NNLO ($\overline{\text{MS}}$)				
	u_v	d_v	$\bar{d} - \bar{u}$	$\bar{u} + \bar{d}$	g
N	4.4049	13.824	8.6620	1.2316	23.034
a	0.7875	1.1778	1.2963	0.1374	0.9940
b	3.6857	5.6754	19.057	10.843	6.7892
A	-1.1483	-2.2415	-6.8745	-4.5634	-
B	4.5921	3.5917	19.402	11.940	-
χ^2/dof	0.986 (0.904)				
$\alpha_s(M_Z^2)$	0.1124 ± 0.0020				

Table 1: Parameters of our dynamical input distributions as parametrized in (17) referring to an input scale of $Q_0^2 \equiv \mu_{\text{NNLO}}^2 = 0.55 \text{ GeV}^2$. Since the gluon distribution turned out to be insensitive to the polynomial terms in (17), we have set them to zero ($A_g = B_g = 0$). The total numbers of degrees of freedom is $\text{dof} = 1568 - 21 = 1547$. The χ^2/dof in brackets refers just to the DIS data where $\text{dof} = 1178 - 21 = 1157$. Furthermore $\alpha_s(\mu_{\text{NNLO}}^2)/\pi = 0.1522$.

	NNLO ($\overline{\text{MS}}$)				
	u_v	d_v	$\bar{d} - \bar{u}$	$\bar{u} + \bar{d}$	g
N	3.2350	13.058	8.1558	0.4250	3.0076
a	0.6710	1.0701	1.1328	-0.1098	0.0637
b	3.9293	6.2177	21.043	10.341	5.4473
A	-0.5302	-2.5830	-7.6334	-3.0946	-
B	3.9029	3.8965	20.054	11.613	-
χ^2/dof	0.947 (0.873)				
$\alpha_s(M_Z^2)$	0.1158 ± 0.0035				

Table 2: As Table 1 but for the input parameters in (17) of the standard fit at an input scale $Q_0^2 = 2 \text{ GeV}^2$, where $\alpha_s(Q_0^2)/\pi = 0.1072$.

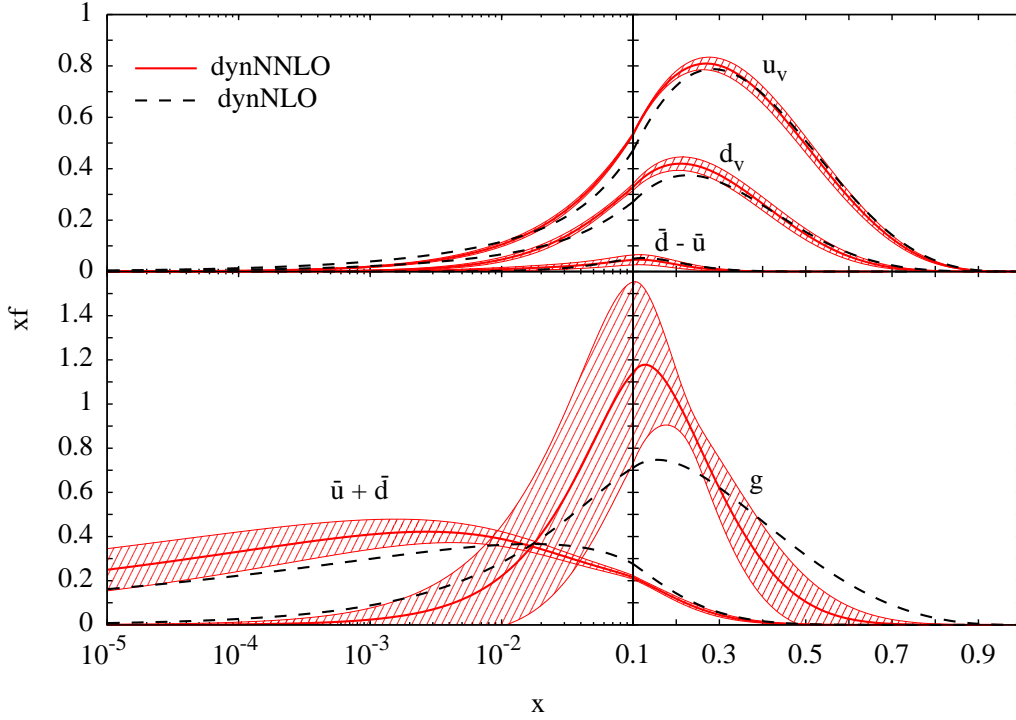


Figure 1: The dynamical NNLO valence ($u_v, d_v, \bar{d} - \bar{u}$) and valence-like ($g, \bar{u} + \bar{d}$) input distributions together with their $\pm 1\sigma$ uncertainties at $Q_0^2 \equiv \mu_{\text{NNLO}}^2 = 0.55 \text{ GeV}^2$. The central curves follow from (17) with the parameters given in Table 1. The strange sea $s = \bar{s}$ vanishes at the input scale. Our dynamical NLO input [8] at $Q_0^2 \equiv \mu_{\text{NLO}}^2 = 0.5 \text{ GeV}^2$ is also shown by the dashed curves for comparison. The 1σ uncertainties at NLO [8] are comparable to the ones shown at NNLO, except for the NLO gluon at $x \gtrsim 0.3$ which is stronger constrained due to the light high- p_T jet data [8].

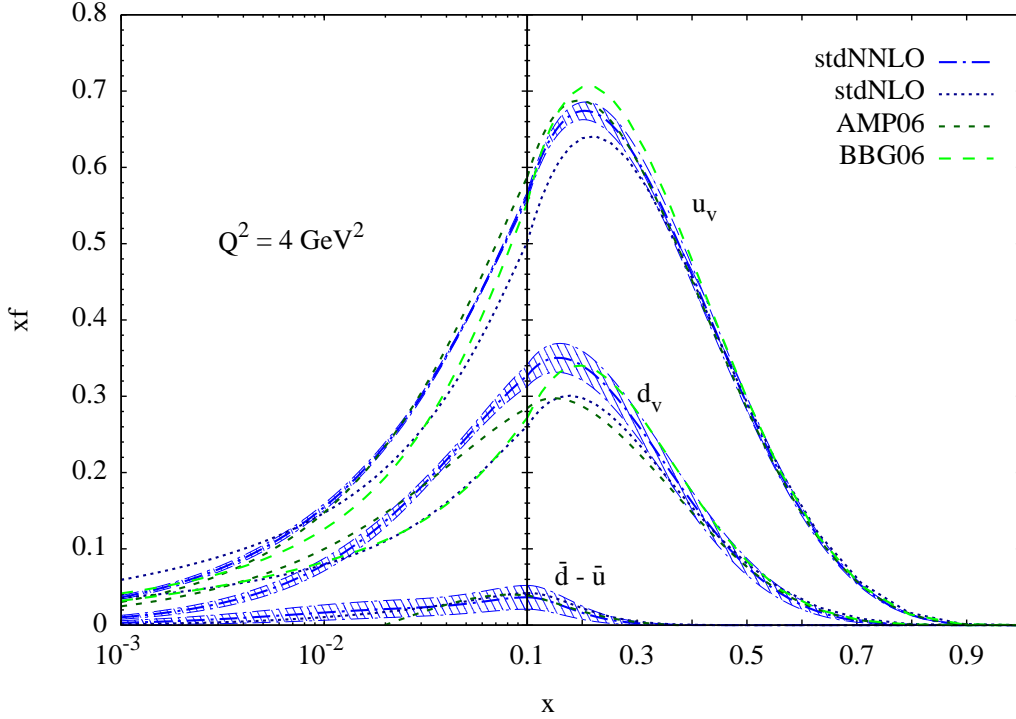


Figure 2: Our standard NNLO valence distributions together with their $\pm 1\sigma$ uncertainties at $Q^2 = 4 \text{ GeV}^2$, according to the input parameters in Table 2 at $Q_0^2 = 2 \text{ GeV}^2$ for the central curves. Our standard NLO results [8] are shown by the dotted curves. For comparison the standard NNLO results of AMP06 [17] and BBG06 [87] are shown as well. Our dynamical valence distributions at $Q^2 = 4 \text{ GeV}^2$ practically coincide with the standard ones shown.

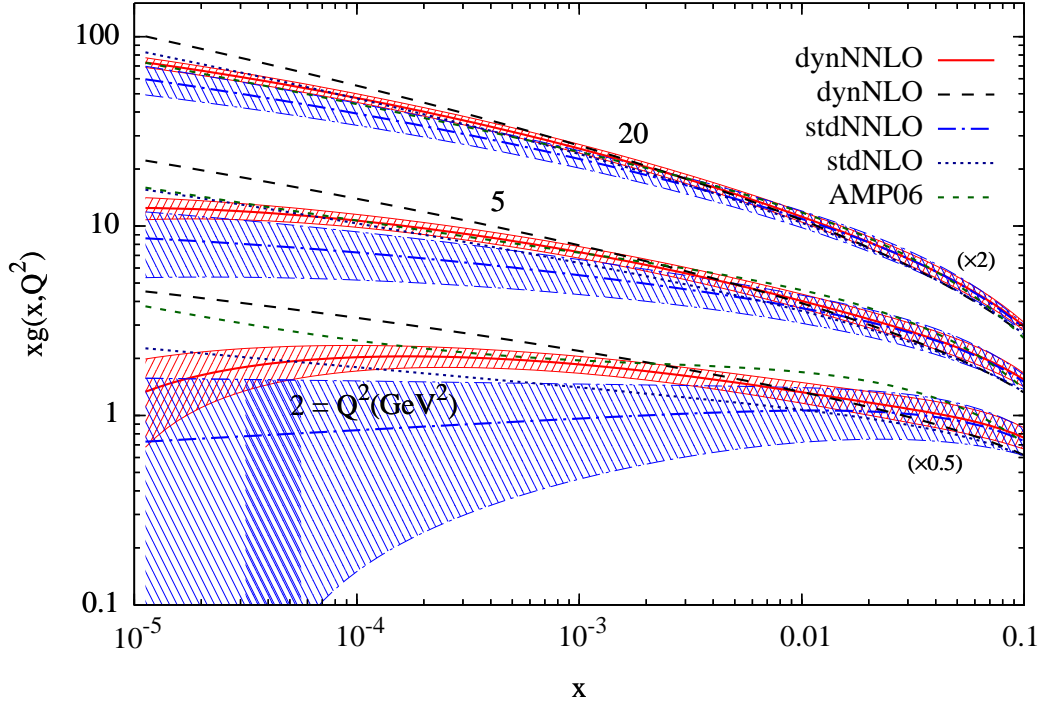


Figure 3: Comparing the $\pm 1\sigma$ error bands of our dynamical (dyn) and standard (std) NNLO gluon distributions at small x for various fixed values of Q^2 . Note that $Q^2 = 2 \text{ GeV}^2$ is the input scale of the standard fit. The central NLO results are taken from [8] with uncertainties comparable to the ones shown for NNLO for Q^2 above 2 GeV^2 . For comparison the ‘standard’ NNLO results of AMP06 [17] are shown as well. The results at $Q^2 = 2$ and 20 GeV^2 have been multiplied by 0.5 and 2 , respectively, as indicated in the figure.

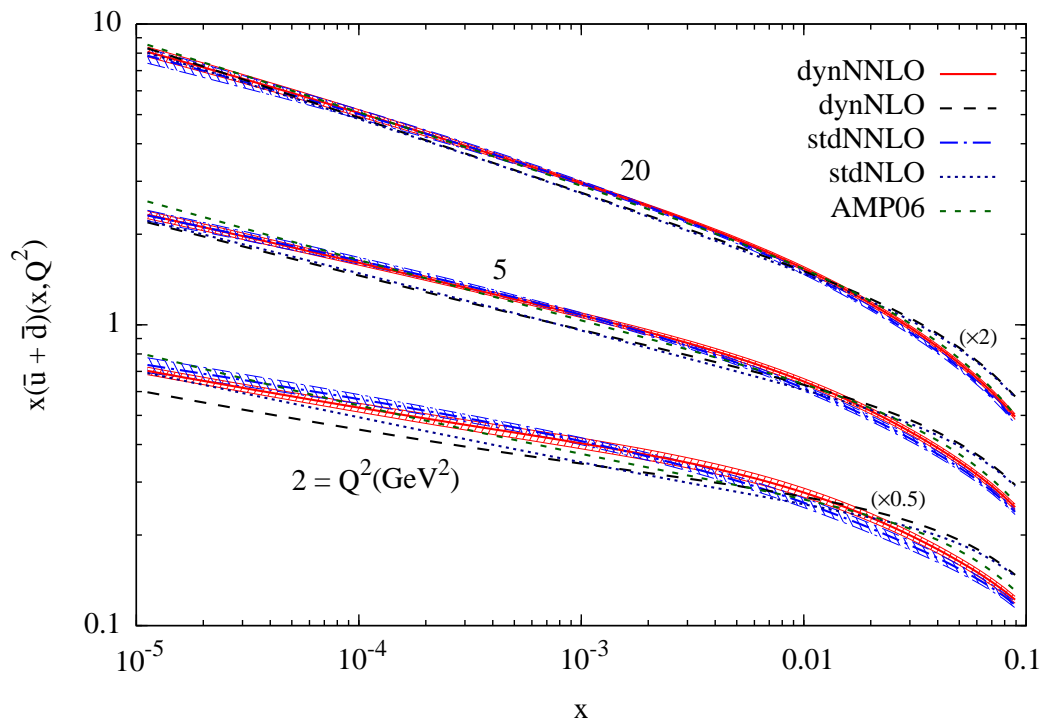


Figure 4: As in Fig. 3 but for the sea quark distribution $x(\bar{u} + \bar{d})$.

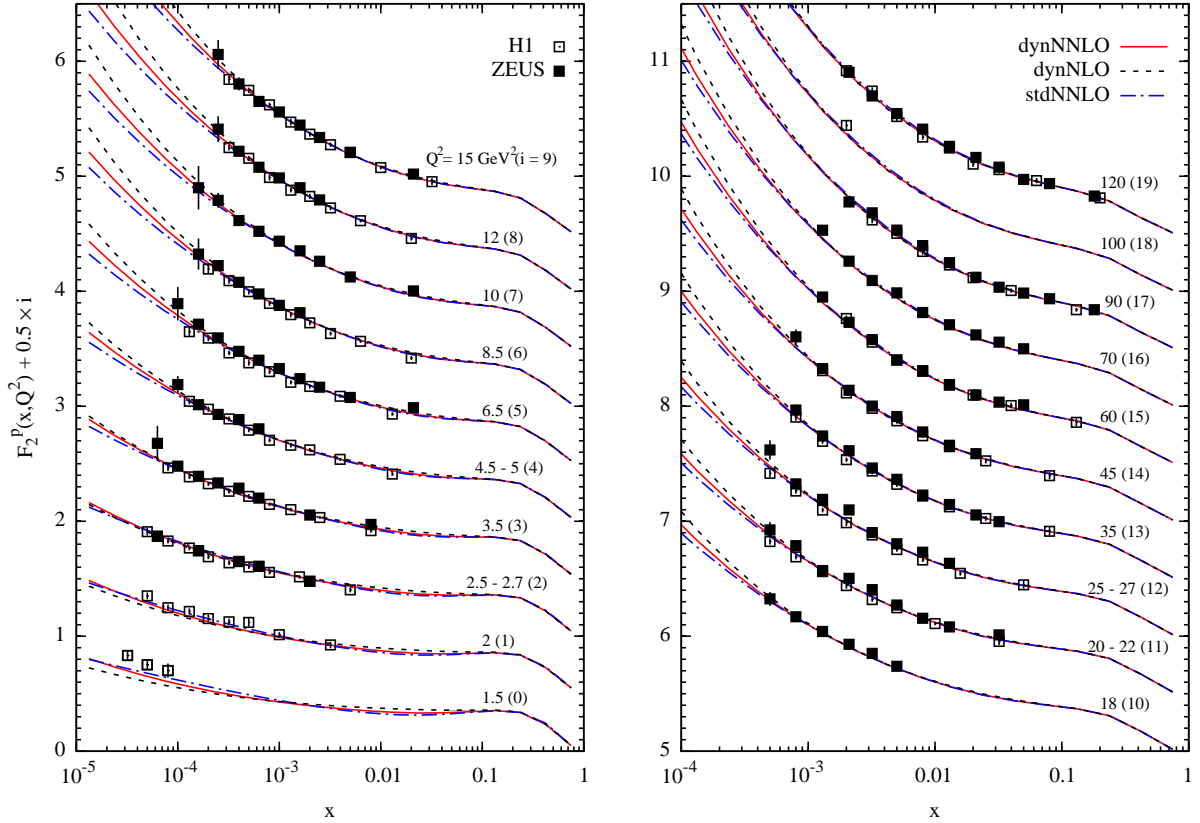


Figure 5: Comparison of our dynamical (dyn) and standard (std) NNLO small- x results for $F_2^p(x, Q^2)$ with HERA data for $Q^2 \geq 1.5 \text{ GeV}^2$ [70–74]. The dynamical NLO results are taken from [8]. To ease the graphical presentation we have plotted $F_2^p(x, Q^2) + 0.5i(Q^2)$ with $i(Q^2)$ indicated in parentheses in the figure for each fixed value of Q^2 .

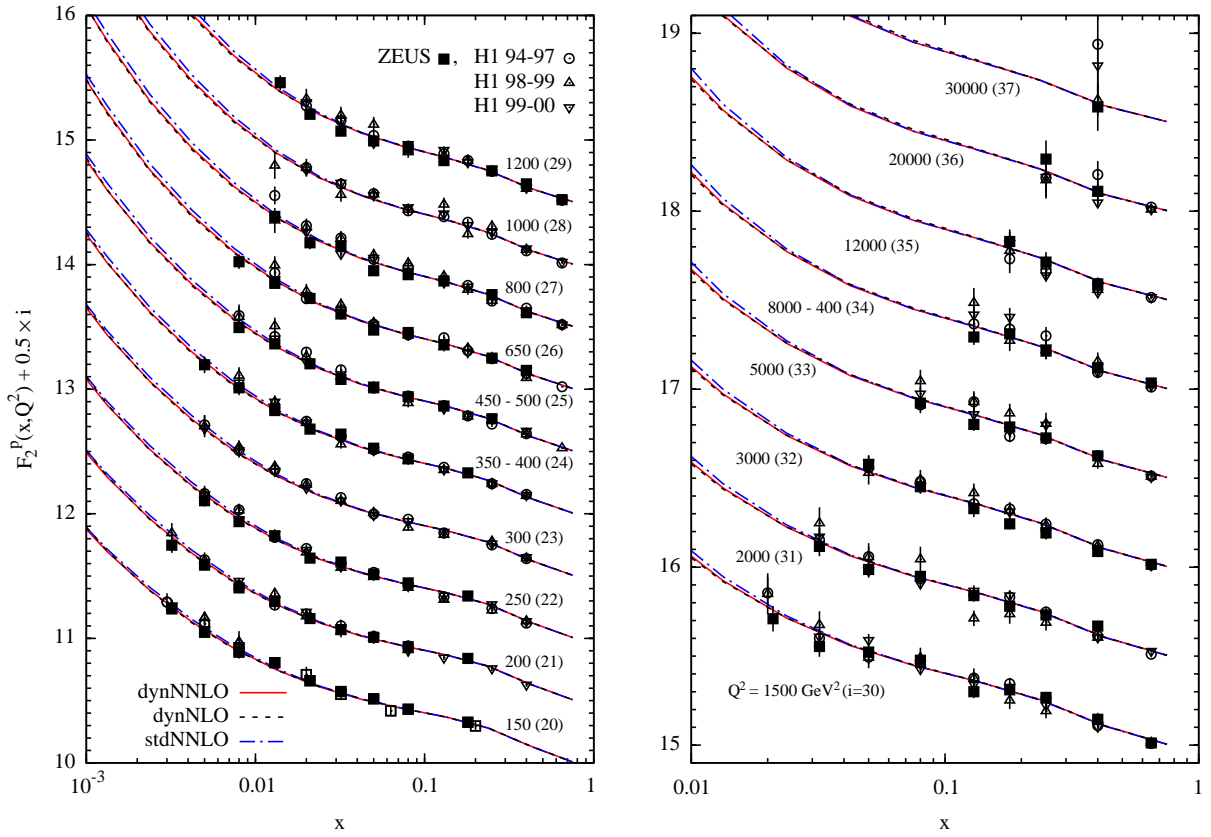


Figure 6: As in Fig. 5 but for large values of Q^2 and larger x .

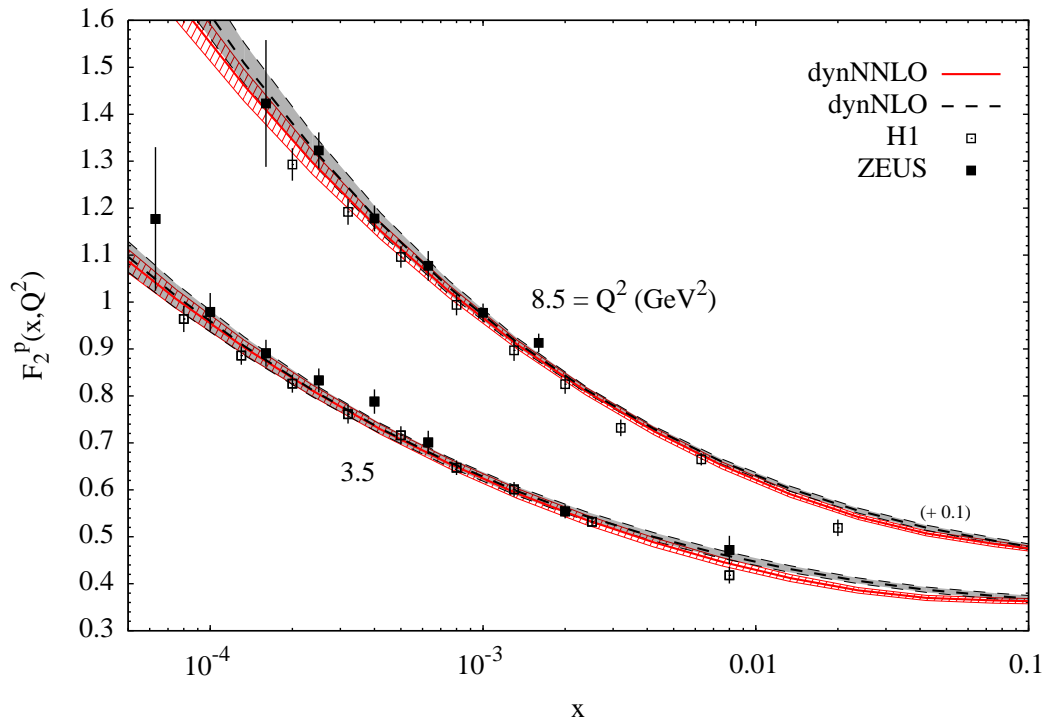


Figure 7: Typical $\pm 1\sigma$ uncertainty bands of our dynamical NNLO and NLO results in Fig. 5 for two representative values of Q^2 . The ‘standard’ NNLO and NLO results are very similar. To ease the visibility we have added 0.1 to the results for $Q^2 = 8.5 \text{ GeV}^2$ as indicated.

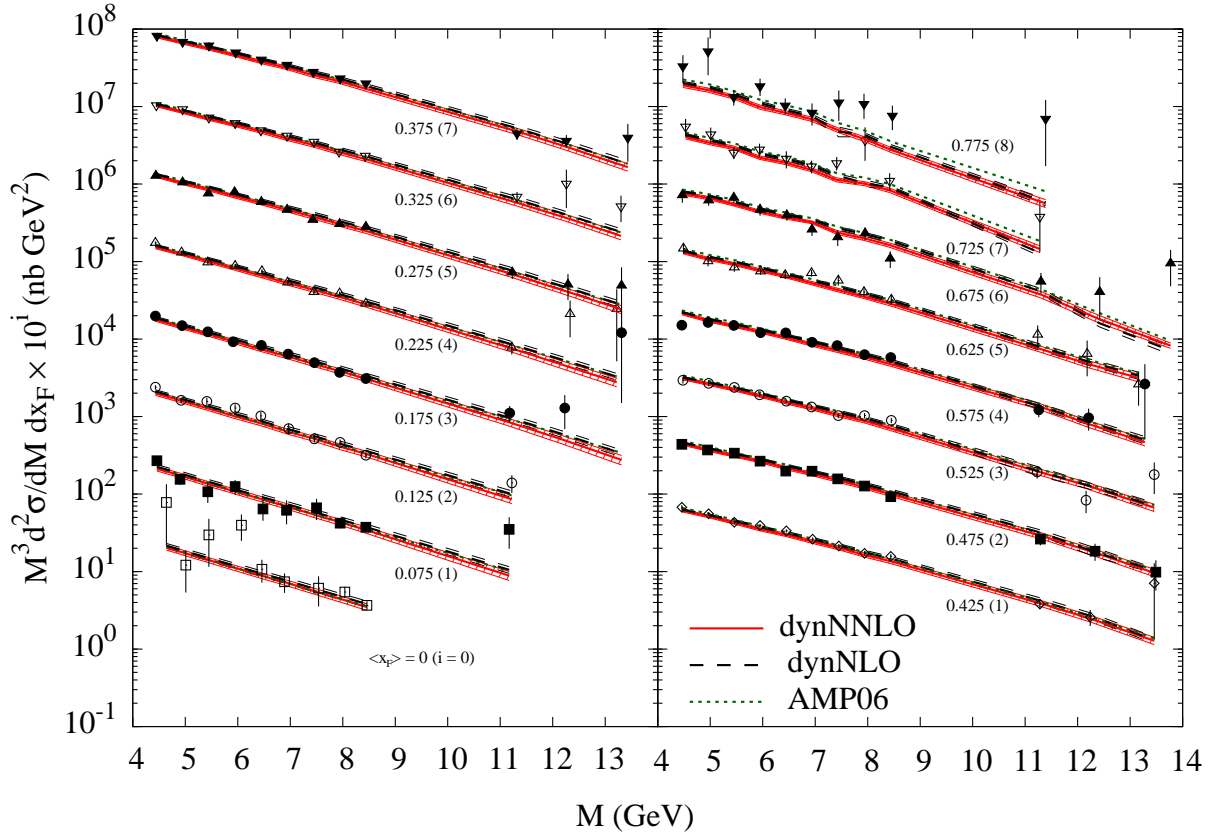


Figure 8: Our dynamical NNLO and NLO [8] results, together with their $\pm 1\sigma$ uncertainties, for Drell–Yan dilepton production in pp collisions for various selected average values of x_F using the data sets of [82]. For comparison the NNLO AMP06 results [17] are shown as well. To ease the graphical presentation we have multiplied the results for the cross sections by 10^i with i indicated in parentheses in the figure for each fixed average value of x_F .

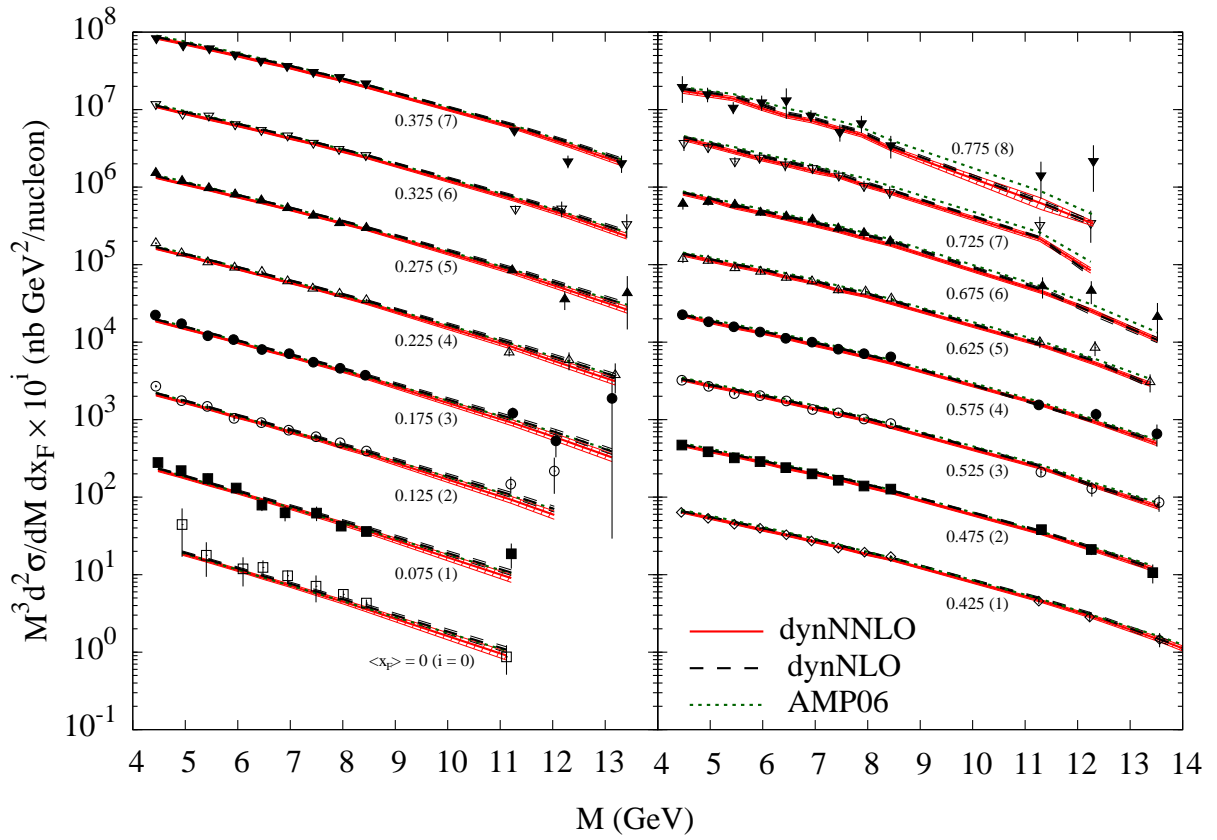


Figure 9: As in Fig. 8 but for pd collisions.

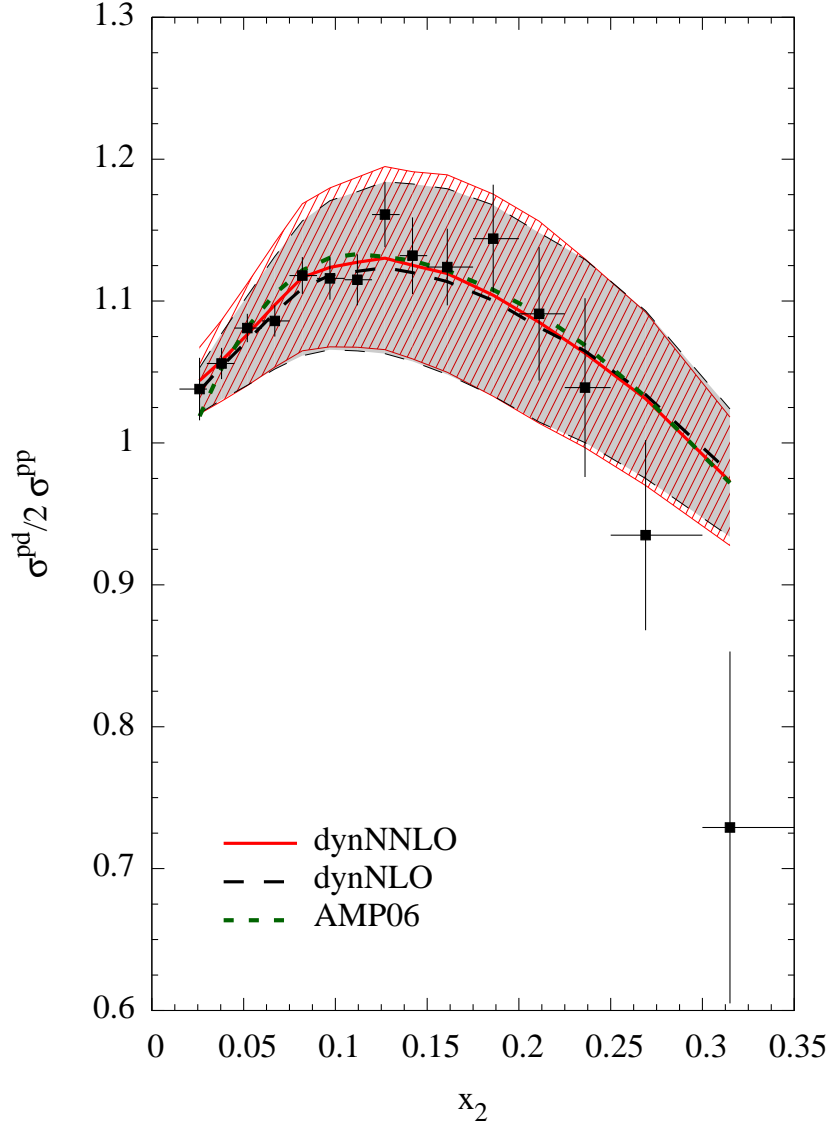


Figure 10: Our dynamical NNLO and NLO results, together with their $\pm 1\sigma$ uncertainties, for $\sigma^{pd}/2\sigma^{pp}$ as a function of the average fractional momentum x_2 of the target partons. The dynamical NLO results are taken from [8], and the NNLO AMP06 ones from [17]. The data for the dimuon mass range $4.6 \text{ GeV} \leq M \leq 12.9 \text{ GeV}$ are from [83].

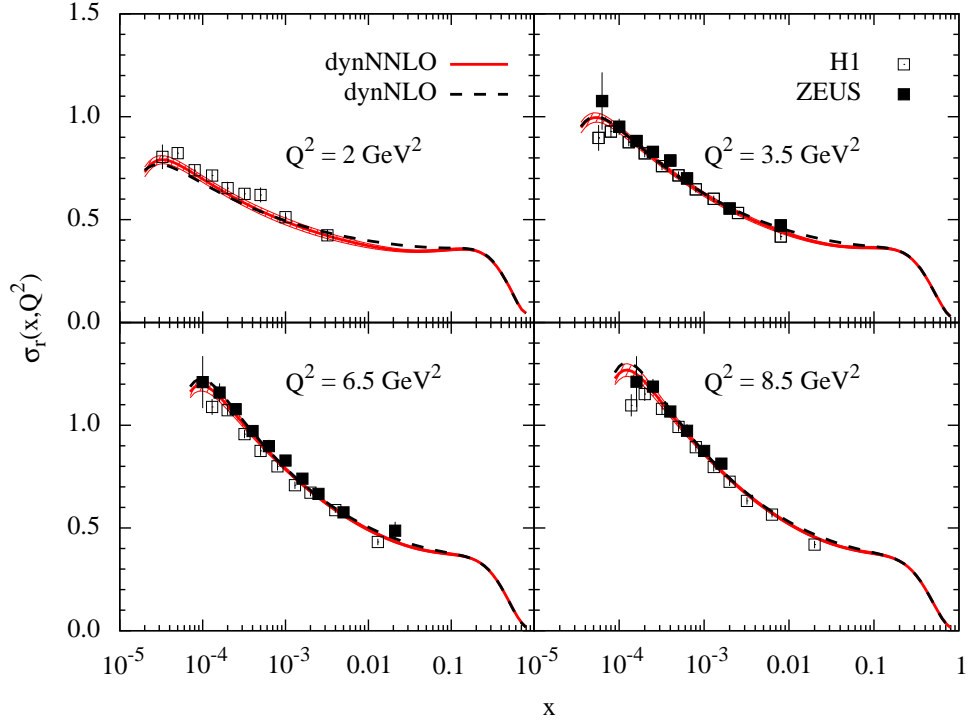


Figure 11: The dynamical NNLO predictions, together with their $\pm 1\sigma$ uncertainties, for the ‘reduced’ DIS cross section $\sigma_r(x, Q^2) = F_2 - (y^2/Y_+)F_L$. The uncertainty bands of our previous dynamical NLO results (dashed curves) are very similar in size [8] as the ones shown for NNLO. The HERA data for some representative fixed values of Q^2 are taken from [70–74].

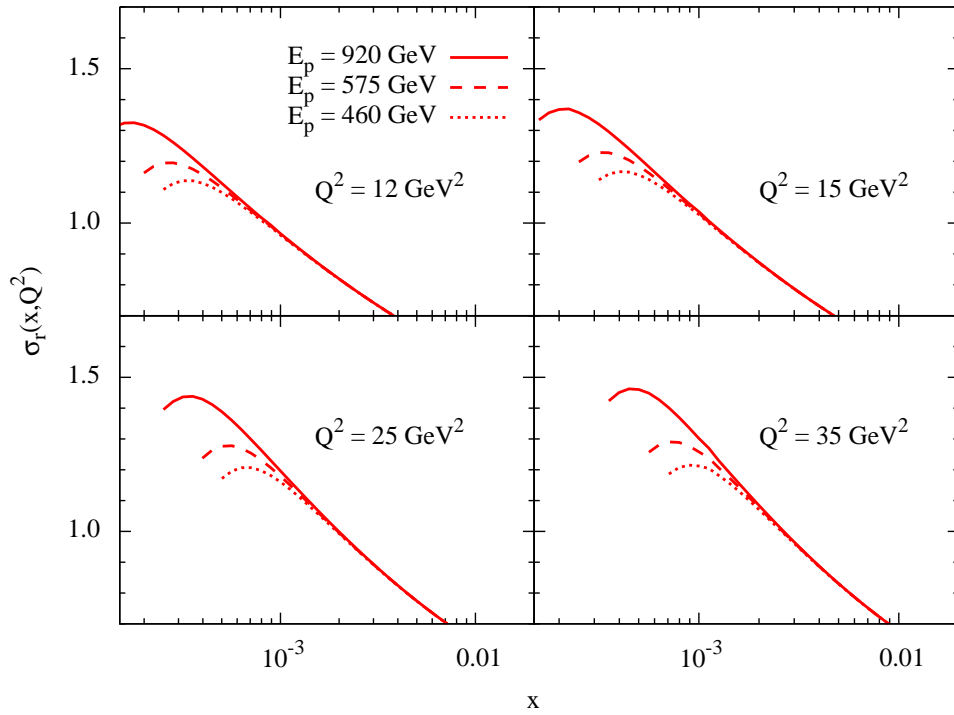


Figure 12: Our dynamical NNLO predictions for $\sigma_r(x, Q^2)$ but for different proton beam energies E_p relevant for most recent HERA–H1 measurements [96]. The $\pm 1\sigma$ uncertainty bands are similar to the ones shown in Fig. 11. Notice that the curves terminate when $y = 1$.

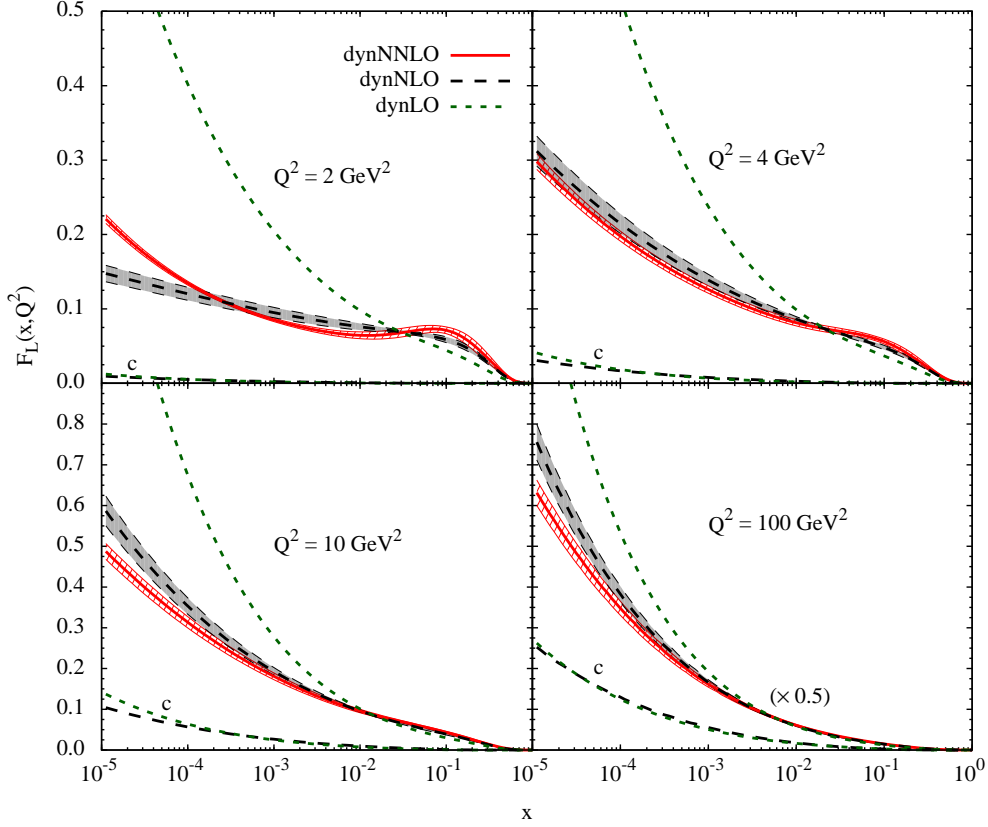


Figure 13: Dynamical parton model LO, NLO and NNLO predictions for $F_L(x, Q^2)$ together with the $\pm 1\sigma$ uncertainty bands at NLO and NNLO. The heavy charm (c) contributions at LO (short-dashed curves) and NLO (long-dashed curves) are shown as well. The results at $Q^2 = 100 \text{ GeV}^2$ are multiplied by 0.5 as indicated.

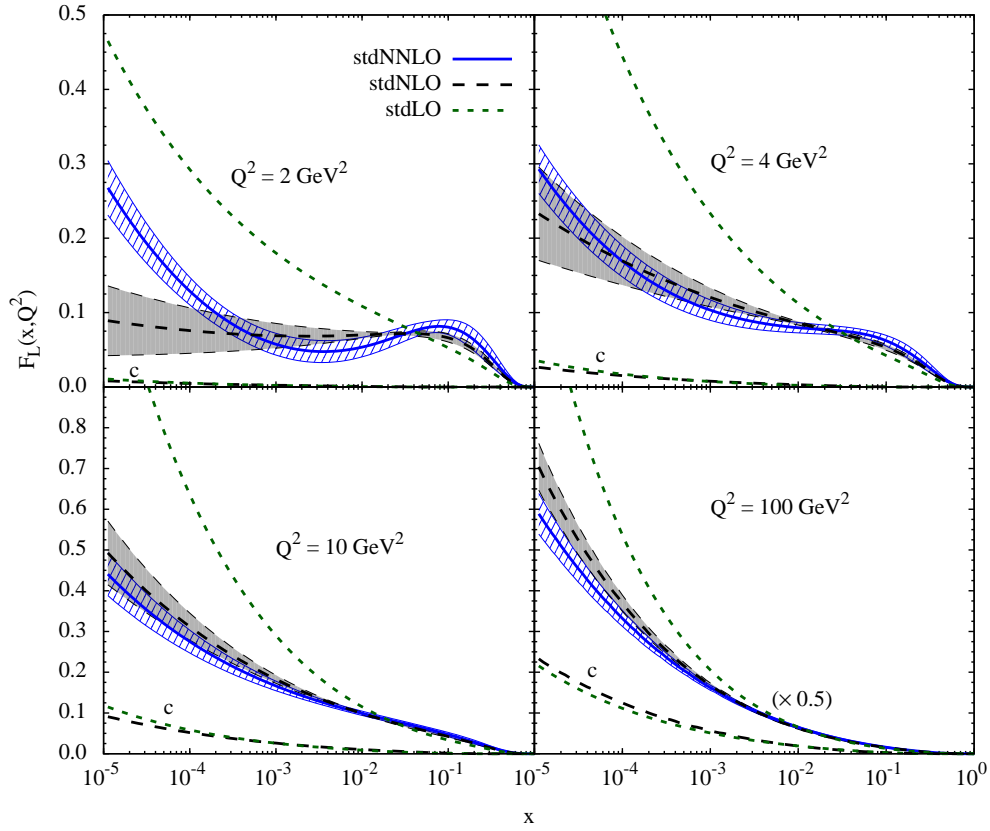


Figure 14: As in Fig. 13 but for the common standard parton distributions. Note that $Q^2 = 2 \text{ GeV}^2$ coincides here with the input scale Q_0^2 .

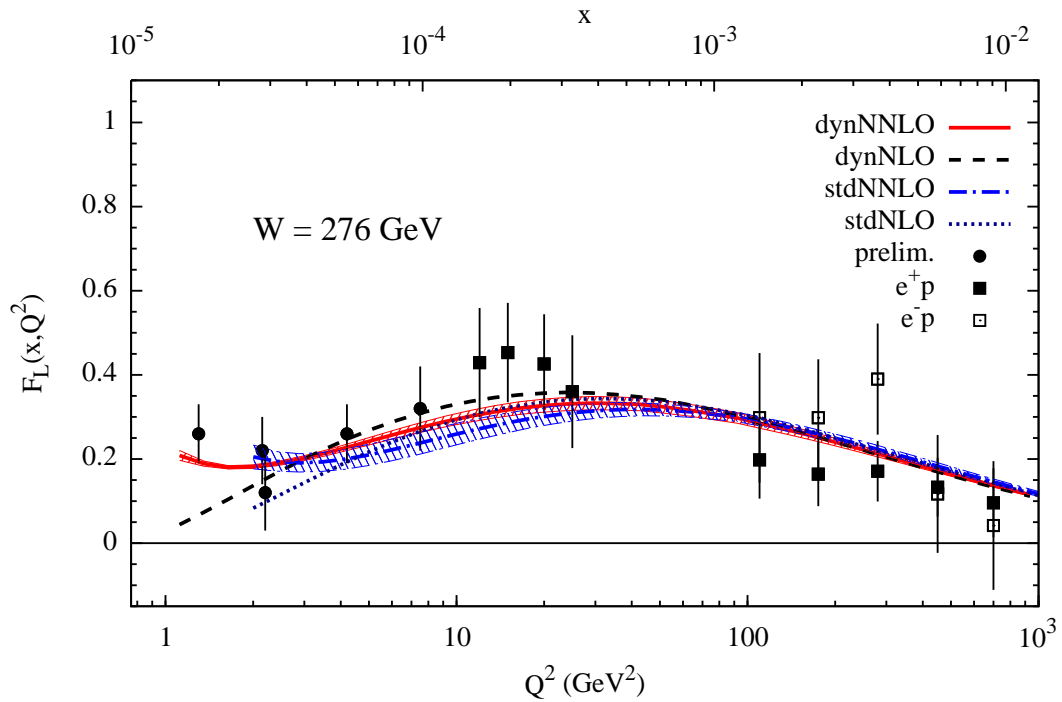


Figure 15: Dynamical and standard NNLO and NLO predictions for $F_L(x, Q^2)$ at a fixed value of $W = 276$ GeV. The NLO($\overline{\text{MS}}$) results are taken from [8]. The (partly preliminary) H1 data [72, 73, 101, 102] are at fixed $W \simeq 276$ GeV. The more recent H1 data [96], which correspond to smaller values of W (larger x and Q^2), are compatible with the indirectly determined data shown.